Nigerian Journal of Physics (NJP)
ISSN online: 3027-0936
ISSN print: 1595-0611
DOI: https://doi.org/10.62292/njp.v35i4.2026.654
Volume 35(4), December 2026

Porosity and Geomechanical Characteristics of banded Iron Ore from Itakpe, North Central Nigeria

*[1,2]Ige-Adeyeye A. Amidu, [1]Olatinsu B. Olawale, [1]Ozebo C. Vitalis and [3]Esteban Lionel

[1]Department of Physics, University of Lagos, Akoka, Yaba, Lagos, Nigeria.
[2]Department of Physical Science, Lagos State University of Science and Technology, Ikorodu, Lagos, Nigeria.
[3]CSIRO-Energy, Oil, Gas and Fuels Program, 26 Dick Perry Avenue, Kensington, 6151, Perth, Australia.

*Corresponding Author's Email: ige-adeyeye@lasustech.edu.ng

Keywords:
Itakpe iron ore,
Porosity,
Uniaxial compressive strength,
Elastic modulus,
Modulus ratio.

Submitted: 17 Jul. 2026

Accepted: 24 Jul. 2026

Published: 27 Jul. 2026

ABSTRACT

The microstructural characteristics of geological materials are fundamentally influenced by their pore configuration and geomechanical properties. The banded iron ore samples from Itakpe, North Central Nigeria, have been examined using: (i) X-ray fluorescence (XRF) spectroscopy for preliminary iron content assessment; (ii) low-field nuclear magnetic resonance (NMR) and water imbibition porosity (WIP) techniques for pore structure evaluation; and (iii) bulk density and stress-strain analysis for the geomechanical characterisation. The average weight of haematite, silica, alumina and iron contents in the samples are 53%, 22%, 12%, and 37%, respectively. These values show that the Itakpe iron ores are low-grade and hence, significant enrichment is required for economic viability. The pore system of the ore samples is basically bimodal without any indication of macropores, in agreement with the metasedimentary origin of the ores. The transverse relaxation time ranges for the pore regions are: (a) micropores (0.2818 – 1.413 ms) and (b) mesopores (7.943 – 79.43 ms). The mean porosities estimated via NMR and WIP techniques are 0.365 p.u. and 0.488 p.u., respectively. Computed porosity and water content from NMR and WIP techniques show high degree of correlation which are 87% and 76%, respectively. The average UCS, elastic modulus and dry bulk density of the samples are 101.28 MPa, 3.94 GPa and 3.46 g/cm^3, respectively showing high strength ores. The plots of UCS versus dry bulk density for the samples shows an increasing exponential relation, while the UCS versus NMR porosity, modulus ratio versus dry bulk density as well as modulus ratio versus UCS all show decreasing exponential relations. The UCS is negatively correlated with NMR porosity but positively correlated with bulk density. Integrating NMR and geomechanical techniques can reliably: (i) predict mechanical behaviour without destructive testing; (ii) complement traditional porosity methods; and (iii) assist in mine design for safety and ore optimisation.

INTRODUCTION

Iron ore and its derivatives are undoubtedly the most economically and historically significant commodities globally after oil and gas (Jégourel, 2020; Holmes et al., 2022; Küblböck et al., 2022). This is partly due to the fact that steel, the major byproduct (about 98%) of iron ore, is the bedrock of industrial revolution and a key driver of global transformation and modern development (Madureira, 2012; Holmes, 2013; Holmes & Lu, 2015). Iron ore is found in igneous, sedimentary and metamorphic rocks, majorly as iron oxides and hydroxides (haematite and magnetite) (Santoro et al., 2022; Gareev, 2023). However, iron content is often low in most iron ore deposits. Thus, an "ore grade" deposit must contain a high concentration of iron for economic consideration (Holmes et al., 2022; Isah & Aliyu, 2024). This implies that in many cases, significant processing to improve ore grade through beneficiation may be necessary. Therefore, the value of iron ore is largely dependent on its iron content as well as the processing procedures (Upadhyay et al., 2010; Bett & Maranga, 2012).

Global iron ore deposits include the vast Banded Iron Formations (BIFs), found in very significant quantities in Australia, Brazil, and India. Other types are the magmatic deposits and oolitic ironstones, with largest reserves in Australia, Brazil, Russia, and China (Beukes et al., 2003; Kholodov & Butuzova, 2008). Significant iron ore deposits are also found in West Africa (Guinea, Liberia, Nigeria and Mauritania), Southern Africa (South Africa and Zimbabwe) and North Africa (Morocco, Tunisia and Egypt) (Foster, 2023). In Nigeria, BIF occurs in folded bands and lenses in the Precambrian metasedimentary schist belts with recognisable outcrops in the North Central and Northwestern zones (Oyedele et al., 2016). The Cretaceous sedimentary (oolitic) iron deposits occur mainly in the North Central, Southeastern and Southwestern zones (Oyedele et al., 2016). The Itakpe iron ore deposit with a total estimated reserve of about 200 million metric tonnes consists mainly of quartzite with magnetite and haematite with about 36% Fe (Akinrinsola & Adekeye, 1993; Olade, 2019; Afeni et al., 2020). The deposit has been developed for supply of iron ore concentrates to Ajaokuta steel plant and the Delta steel plant, Aladja (Akande et al., 2020).

Laboratory analysis of iron ores is important in the integral mining, exploration and processing stages. The various laboratory procedures (geochemical, petrophysical and geomechanical) are able to provide critical data that guides decision-making, ensures economic viability, and guarantees the quality of end products. Data and deductions from these techniques helps to determine the most efficient extraction and processing techniques. Geochemical analysis assists in the evaluation of the iron content and identification of impurities like silica and sulphur, etc. A good understanding of the pore characteristics of iron ore is necessary for performance evaluation during processing. This aspect of pore assessment is often neglected while focus is usually placed on the analysis of chemical composition and impurity contents. Geomechanical analysis usually provides valuable insights on the behaviour of ores (rocks) under stresses induced by excavation and comminution and/or ore breakage (Shah et al., 2020; Way et al., 2021; Pereira et al., 2023). This is vital for safety, optimisation of mine design, efficiency and optimal resource recovery. Comminution in particular, accounts for a significant portion of processing costs, hence, its implementation demands high efficiency (King, 1994; Bradshaw, 2014; Zuo & Shi, 2016; Klein et al., 2018; McNulty et al., 2022). Furthermore, the microstructure of rocks (pore sizes, shapes, pore throats, fractures/cracks, mineral inclusions/impurities in the rock matrix, porosity, etc.) and their changes during mechanical stressing is essential in comminution process (Armstrong et al., 2009; Zhang et al., 2010; Anovitz and Cole, 2015; Li et al., 2018; Xu et al., 2020; Salvini et al., 2023 Tavares, 2000; Liu et al., 2024). Thus, rock microstructures are presumed to have considerable effect on many mechanical properties such as particle breakage which predicts macroscopic damage behaviour in comminution process (Rust & Cashman, 2011; Sparks et al., 2019; Pereira et al., 2025). In addition, ore breakage is often facilitated by the connectivity of pores within rocks, as well as by the presence of inherent cracks due to their geological history (Wills & Atkinson, 1993; Bevilacqua & Ferrara, 1996; Kuila & Prasad, 2013; Pereira et al., 2025; Korbel et al., 2026).

Nuclear magnetic resonance (NMR) techniques provide valuable insights on the flow properties in the pore spaces of rocks, porosities, pore size distribution, etc. (Blümich et al., 2009; Grunewald & Knight, 2011; Yao and Liu, 2012; Olatinsu et al., 2017; Yao and Liu, 2019; Benavides et al., 2020; Feng et al., 2020; Wang et al., 2020; Golsanami et al., 2021; Downey et al., 2024). Several techniques for pore characterisation of rock and minerals exist, with each method having a unique principle and scope of application. These include thin section identification, mercury intrusion porosimetry (MIP), gas adsorption, computerized tomography (CT), scanning electron microscopy (SEM) etc. However, all these methods are often limited to qualitative or semiquantitative information on sample compositions and pores. NMR technique has the potential of full-scale quantitative description of pore characteristics. It offers significant advantages over other methods due to its non-destructive nature, wider pore size range detection, and minimal sample preparation requirements. The porosity and geomechanical properties of iron ores are highly variable and fundamentally linked; porosity significantly influences their strength, density, and behaviour during mining and processing. Geomechanical properties predict the response of a rock or geomaterial under stress and hence, are very relevant for safe and efficient mining and processing design. High porosity enhances comminution by reducing the mechanical strength of a rock, facilitates disintegration into smaller particles and changes the resulting size distribution (Anovitz & Cole, 2015; Somani et al., 2017; Zhu et al., 2025). Besides reducing energy consumption for comminution due to lower compressive strength and stiffness, higher porosity in rocks can also introduce pore-related breakage mechanisms that can result in distinct multi-modal pore size distributions (Jin et al., 2021; Pamparana et al., 2024). Thus, the knowledge of the relationships between petrophysical properties (porosity, pore sizes, moisture content, water saturation, permeability, etc.) and geomechanical characteristics (dry bulk density, tensile strength, uniaxial compressive strength, shear strength, elastic modulus, modulus ratio, Poisson's ratio, etc.) can assist in predicting the response of ores to stress during mining, crushing, and transportation (Jeng et al., 2004; Ulusay, 2015; Bello & Onifade, 2016; Atapour &

Mortazavi, 2018a, 2018b; Dalirnasab et al., 2024). Several workers have established the connection between rock strength and pore structure, porosity, fracture and constituent heterogeneity (Palchik, 2011; Siegesmund & Dürrast, 2011; Khanlari et al., 2014; Zhang & Zhao, 2014; Ulusay, 2015; Li et al., 2019; Liu et al., 2024).

Uniaxial compressive strength (UCS) is a physical property of rocks for strength characterisation and is relevant to iron ore crusher design and rock geomechanics for mining. It is also widely used in engineering design and stability analysis, rock mass classification, and geomechanical modelling (Gholami & Fakhari, 2017; Xie et al., 2025; Yang et al., 2025; Ju et al., 2024; Xie et al., 2025). Porosity plays a significant role in the geomechanical parameters of rock. Several inverse relationships have been established between some geomechanical properties and porosity of rocks/ores (Chindaprasirt et al., 2009). Porosity and rock strength are inversely related: increase in total porosity or the formation of large pores typically reduces mechanical strength, and can lead to potential breakage during handling and transport (Ryshkewitch, 1953). In essence, understanding the intrinsic variation and connection between porosity and geomechanical properties is vital for managing the quality, safety, and efficiency of iron ore operations, from mine planning to final processing. Studies have shown that the UCS of volcanic rock decreases as the total porosity increases (Ündül, 2012) but the presence of micro-cracks and discontinuities can lower overall strength (Peng et al., 2019; Han et al., 2022; Zhai et al., 2025). Bell and Lindsay (1999) reported that UCS and tensile strength decrease as porosity increases. Some sets of equations which connect the petrophysical to the geomechanical properties of the basement rocks of the Krishna-Godavari and Cauvery Basins in India have been developed (Chatterjee and Mukhopadhyay, 2008). Therefore, the knowledge of porosity and geomechanical characteristics of iron ores is very important: for efficient extraction process, increase resource recovery, comminution efficiency and ore characteristics under different stress conditions (Niu & Zhang, 2018; Dalirnasab et al., 2024). This study examines the porosity and/or pore structure and geomechanical characteristics of Itakpe iron ore using water imbibition porosity (WIP) and low-field NMR techniques, and stress-strain analysis. The objectives are to provide valuable data and relations that are useful for primary consideration in beneficiation and comminution process of Itakpe and other global iron ore deposits and by extension for wider considerations in geotechnical engineering, rock mechanics, and mining geotechnics.

Geological Environments

The geology of Nigeria is characterized by three primary components: the Basement Complex, the Younger Granites, and the Sedimentary Basins. These formations split the country equally into crystalline rock regions and sedimentary layers, endowed with valuable mineral deposits and oil reserves (Tijani, 2023; Alabi et al., 2025). The geology of Kogi State (Figure 1) is slightly complex with two main litho-petrological units: western part, which lies in the Precambrian to Cambrian basement units of North Central Nigeria and eastern part, which lies in the Cretaceous to Recent Sedimentary Basins of Bida and Anambra respectively (Obaje, 2009; Ifediegwu et al., 2019;). The basement complex of Kogi State consists of Migmatite-Gneiss Complex (migmatites, gneisses, and granite-gneisses) of Mesoarchaean to Neoproterozoic age; Metasedimentary and Metavolcanic rocks (schists, marbles, phylites, pelites, amphibolites and quartzites); Older Granites (granites, granodiorites, dolerites, monzonites, charnockites, gabbro and syenites) Neoproterozoic to Early Palaeozoic in age and undeformed acid and basic dykes (muscovite-, tourmaline- and beryl-bearing pegmatites, applites and syenite dykes; basaltic, doleritic and lampropyric dykes) (Olade, 1978; Rahaman & Ocan, 1978; Olade, 1980; Obaje, 2009; Anudu et al., 2014; Olade, 2019). The prevalent lithological units are: pegmatite, granites, biotite, ferruginous quartzites and migmatite gneiss (Faruwa et al., 2021). The main source of iron ore mineralization is the ferruginous quartzite (Olade, 1978; Fadare, 1983; Annor & Freeth, 1985; Amigun & Ako, 2009; Faruwa et al., 2021). Kogi State is host to the five majorly known types of iron ore deposits in Nigeria: ferruginous quartzites; ferruginous schists; magmatic iron ore; sedimentary ironstones and lateritic ironstone. The iron ore deposits are scattered around the Okene-Lokoja-Kabba axis. The exploitable proportion of the iron ore deposits are within the popularly known "Iron Triangle" of Kogi State (Olade, 2019). Most of the known occurrences of ferruginous quartzites are found in the area around Okene-Lokoja-Kabba in Kogi State, although a few similar deposits have been reported outside this area.

The most prominent basement complex deposit of iron ore is at Itakpe, about 10 km northeast of Okene, and other smaller deposits are at: Chokochoko, Ajabonoko, Agbado-Okudu and Tajimi. Itakpe iron ore is a Precambrian ferruginous quartzite occurring within the Archean migmatite-gneiss quartzite suite of the Basement Complex (Olade, 1978, 2019). It comprises the banded layers of migmatites, gneisses, amphibolites, schists and quartzites, intruded by granites, pegmatites and aplite as the ore deposits have been affected by regional metamorphism via folds and faults. The production capacity for the Itakpe mine was projected as 2.2 million tons per annum of concentrate with 63 - 64% iron content for Ajaokuta, and 0.8 million tonnes of super-concentrate with 67 - 68% Fe (Olade, 2019). Principal ore minerals are magnetite and haematite with quartz, biotite and hornblende as gangue minerals, which are recrystallized quartz alongside little amphibole and biotite (Ameh, 2014; Olade, 2019; Adejuwon et al., 2020).

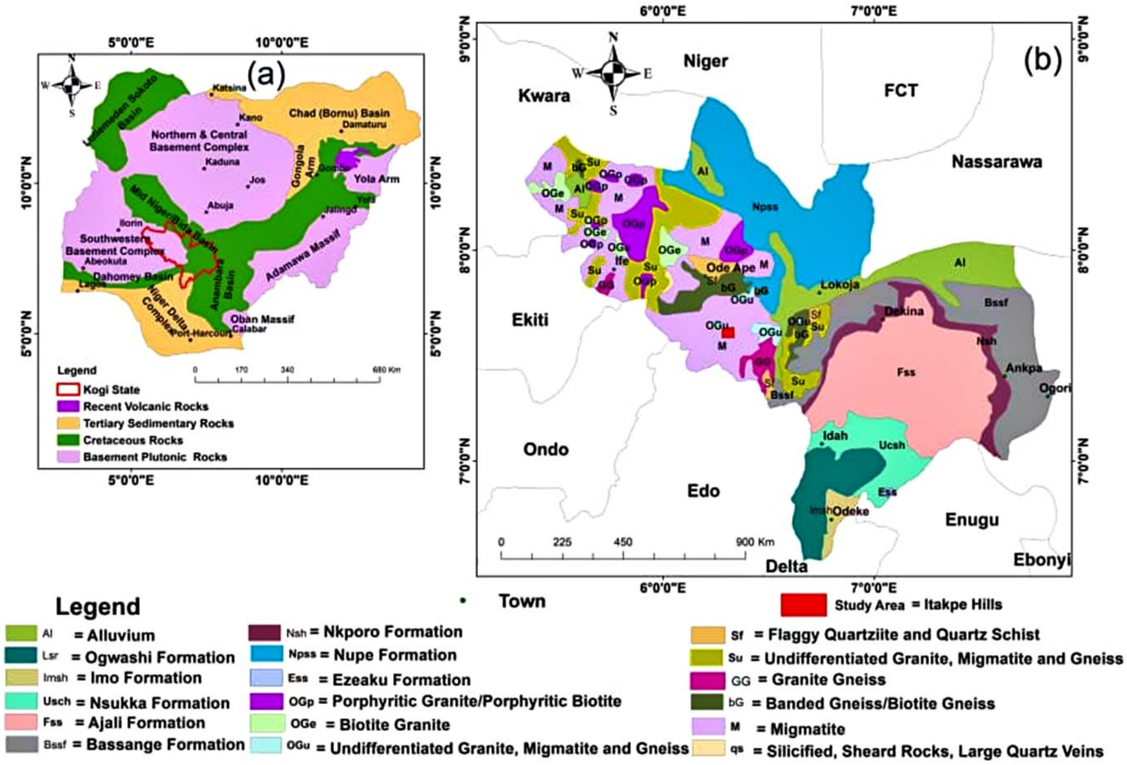

Figure 1: Geological map of: (a) Nigeria showing the location of Kogi State (b) Kogi State showing Itakpe Hills (Modified after Ifediegwu et al., 2019)

The iron ores are banded, massive or schistose, irregular and discontinuous with intercalation of bands of quartz grains. The banded iron formation (BIF) is observed as fine grained pelitic sediments sparsely related to amphibolitic units (Woakes et al., 1987). The Itakpe iron ore deposits consist of ridges which are about 5 km long and 1 km wide, with peaks of about 700 m above sea level (Olade, 1978, 1980). These iron deposits have no apparent genetic relationship to volcanic activity and they are considered as products of high-grade metamorphism of iron-rich sandstones deposited within a platform or epicontinental environment (Olade, 1980).

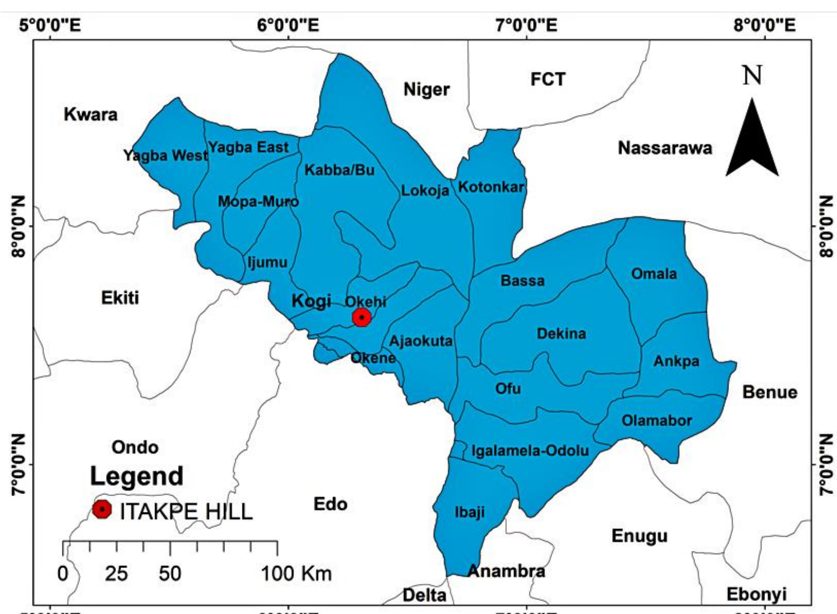

Figure 2: Location of Itakpe Hills in Kogi State, Nigeria

The Itakpe Hills (Figure 2) iron ore deposit lies within latitude 7˚36' 0" – 7˚38' 0" N and longitude 6˚17' 0" – 6˚ 20' 0" E which is 4 km Southwest of Ajabanoko iron ore deposit. It mainly consists of haematite–quartz bodies which is of ferruginous quartzite of the itabirite type (Olade, 1978, 2019). This ferruginous quartzite ore bodies have ore grade ranges between 25 - 55% Fe, averaging about 36% Fe and proven reserves of about 200 million metric tons (Akinrinsola & Adekeye, 1993; Olade, 2019). The Itakpe iron ore is fairly graded and acidified; it is a compact, banded crystalline ore with colour grades varying from grey to black (Adedeji & Sale, 1984).

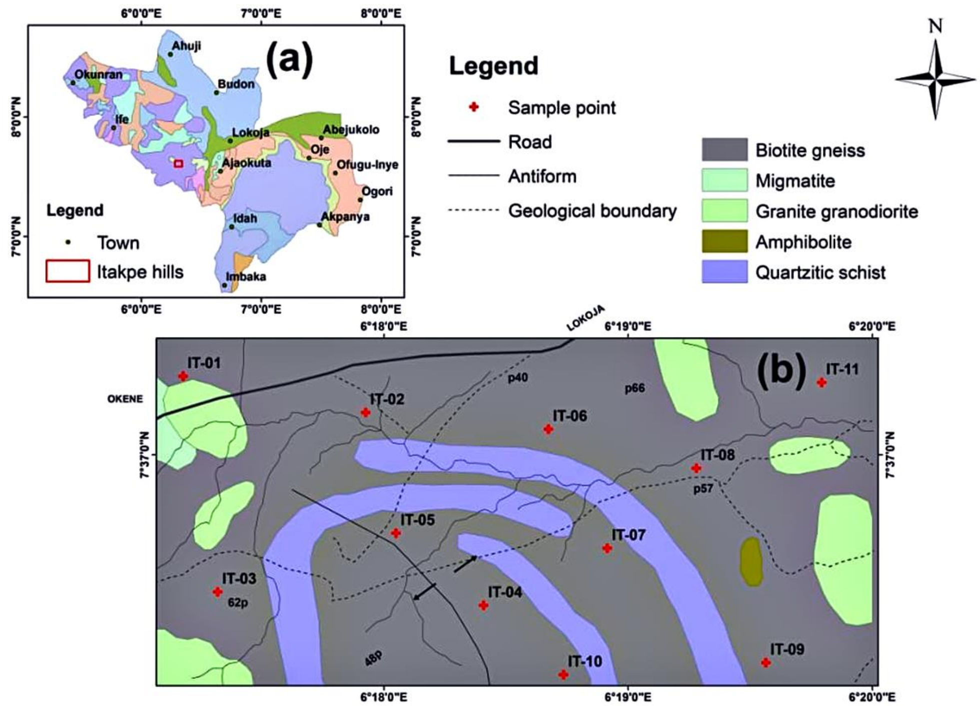

Figure 3: Geological map of: (a) Kogi State (b) Itakpe Hills (Modified after Odigi, 2002)

Low-Field NMR

The proton resonance NMR measurements is a technique in the low-field frequency range (2-100 MHz) of operation (Blümich, 2019). This involves the orientation of magnetic moments of protons by an external magnetic field in a hydrogenous fluid (specifically water) which has partially or wholly saturated the pore spaces of the sample to give a measurable resultant dipole moment (Coates et al., 1999). This technique measures the decay in magnetisation, signal amplitude and relaxation times of spinning protons in the pores of samples influenced by an externally applied magnetic field. The observed magnetisation decay can be deconvolved into spectra of attenuation times: longitudinal (T_1) and transverse relaxation times (T_2) distributions, which carries the same pore information at low frequency and transient pulses (Kleinberg et al., 1993; Kleinberg, 2001; Yao and Liu, 2019). The response of low-field NMR infers the water content of a fully saturated sample, while the signal amplitude denotes the pore volume (Dunn et al., 2002; Casieri et al., 2010; Olatinsu et al., 2017). The transverse relaxation time measurement is better suited for pore structure, fluid typing and permeability determination while the longitudinal time relaxation is crucial in fluid characterisation.

For pores filled with one type of fluid, three mechanisms dictates the measured transverse relaxation time: bulk relaxation (T_{2b}), which is related to the intrinsic relaxation of molecules in each type of fluid; diffusion relaxation (T_{2d}), which influenced by the dynamic behaviour of fluid molecules bearing proton nuclei under gradient fields; and surface relaxation (T_{2s}), which is related to the sample mineralogy and surface-to-volume ratio (S/V) of pores (Kleinberg, 1996; Kenyon, 1997; Coates et al., 1999; Keating & Knight, 2007; Mitchell, 2010; Mondal & Singh, 2023). The transverse relaxation time of protons in porous media pores is given by the equations (1) and (2) (Carr and Purcell, 1954; Meiboom and Gill, 1958):

$$\frac{1}{T_2}=\frac{1}{T_{2b}}+\frac{1}{T_{2s}}+\frac{1}{T_{2d}} \qquad (1)$$

$$\frac{1}{T_2}=\frac{1}{T_{2b}}+\frac{1}{T_{2s}}+\frac{(\gamma G T_E)^2}{12} \qquad (2)$$

where γ is the gyromagnetic ratio, T_E is the time within pulses and G is the magnetic field gradient strength. For low-field, uniform magnetic field (from superconducting magnets) and single-phase saturation of the geological material with a non-viscous fluid (e.g., water), the rate of bulk and diffusion relaxation terms in equation (1) are negligible (Timur, 1969; Kleinberg and Horsfield, 1990; Yao et al., 2010a, 2010b; Keating & Knight, 2012; Ma et al., 2018; Yao et al., 2021). Therefore, the net transverse relaxation rate becomes:

$$\frac{1}{T_2} \approx \frac{1}{T_{2s}} \quad (3)$$

$$\frac{1}{T_2} = \rho_s \left(\frac{S}{V}\right) \quad (4)$$

$$\frac{1}{T_2} = \rho_s \frac{F_s}{r} \quad (5)$$

where ρ_s is the surface relaxivity, which depicts the tendency that the pore surface would bring closer nuclear spins to relaxation; F_s is the pore shape factor, a constant which depends on the geometry of the pore; r is the pore radius.

The NMR-T_2 measurements varies directly with the pore size (with distribution interpreted for a single fluid phase), while the distribution peaks indicate a specific pore environment or type (Grunewald & Knight, 2011; Kleinberg, 2001; Connolly et al., 2019). The total integrated area of NMR-T_2 distribution is proportional to the hydrogen content of the fluid in the pores, which infer its porosity.

MATERIALS AND METHODS

Sample Preparation

Eleven iron ore samples labelled as Itakpe (IT-#) samples were collected from Itakpe Hills, cut into cylindrical shapes and smoothened using grinding machine. Figure 4 shows some samples before and after sample preparation. The diameter and thickness of the cylindrical-shaped iron ore samples range from 4.0 – 4.7 cm and 3.5 – 5.8 cm, respectively. The cored IT-samples were packaged with Ziploc plastic bags to prevent humidity accumulation and transported for NMR measurements at the Commonwealth Scientific and Industrial Research Organization's (CSIRO) NMR laboratory in Perth, Australia. The remaining fragments were retained and packaged separately for the XRF and geomechanical analyses.

Figure 4: (a) Raw iron ore samples from Itakpe; (b) Cylindrical core prepared for laboratory measurements

XRF Acquisition

XRF analysis was aimed at characterising the chemical (elemental oxide) compositions of the Itakpe (IT) iron ore samples. The fragments from each of the core samples were analysed using XRF spectrometer (Phillips PW-1800 – Philips Analytical, Netherland) at Rolab Research and Diagnostic Laboratory, Ibadan, Oyo State, Nigeria. The X-ray equipment used was calibrated with fourteen standard reference materials, with various standard reference materials, each with different focus of the elements of interest. The standard references covered major oxides for which iron oxides, alumina and silica were the oxides of interest in this study as others only occur in traces. 20 g of each sample was crushed, mixed with 0.4 g of stearic acid as binding agent for 1 minute and pulverized at a pressure of 200 kPa for 1 minute by electric crusher and Herzog Gyro-mill (Simatic C7-62, SIEMENS AG, Germany). The Herzog pelletizing equipment produced 32 mm pellet diameter, which were placed in a sample holder of the X-ray equipment for the X-ray fluorescence analysis. The processes were repeated for each sample to improve measurement accuracy.

WIP Acquisition

The WIP acquisition involves porosity measurement of the core samples based on Archimedes' principle (Kuila et al., 2014). The samples were dried in vacuum at 60 ºC till their weights remained unchanged and the dry mass (m_{dry}) and volume (V_{dry}) recorded after cooling in a desiccator to avoid moisture sorption. The IT-samples were then fully saturated in deionized water, and the saturated mass recorded as (m_{sat}). The saturated samples were partially submerged in fresh water and their masses recorded as (m_{sub_sat}). All measurements were repeated to improve accuracy.

The bulk density ρ_b and skeletal density ρ_s of the samples were calculated from equations (6) and (7):

$$\rho_b = \frac{m_{dry}}{m_{sat} - m_{sub\_sat}} \times \rho_w \quad (6)$$

$$\rho_s = \frac{m_{dry}}{m_{dry} - m_{sub\_sat}} \times \rho_w \quad (7)$$

where ρ_w is density of deionized water, Thus, the porosity of the IT- samples measured by the WIP technique (ϕ_{WIP}) is computed using equation (8):

$$\phi_{WIP} = \frac{\rho_s - \rho_b}{\rho_s} \times 100 \quad (8)$$

NMR Acquisition

The eleven IT-samples were sequentially dried for 24 hours at 105 ºC, until each of the sample weights remains unchanged (dry weight), and recorded. Using deionized water and under vacuum condition, the samples were fully saturated via injection for 12 hours. The saturated sample weights were measured and recorded after drying the damped samples with tissue. The NMR equipment (GeoSpec2 2.37 MHz spectrometer with Green Imaging Technologies software (GIT) built-in the system), operating at 21ºC, was calibrated with 3 cm^3 of D_2O/H_2O mix samples for electronic and signal optimisation to the accuracy of ± 0.01 cm^3. Fully saturated samples were subsequently transferred into the NMR equipment for measurements using the Carr-Purcell-Meiboom-Gill (CPMG) sequence (Carr and Purcell, 1954; Meiboom and Gill, 1958). Transverse relaxation time (T_2) data was acquired for each sample by aligning dephased spinning protons via refocusing of its inhomogeneous magnetic field. The multiple echoes in the form of exponentially decaying curves produced the NMR-T_2 distributions after inversion, with digital processing achieved by the GIT software to give the incremental porosities. Further analysis via crossplots was accomplished using MATLAB software. The NMR parameters used for measurements on the samples are given in Table 1.

Table 1: NMR parameters for core samples of Itakpe iron ore

Sample	SNR	Number of Scan (NSA)	NMR Fluid Volume x 10^{-3} (mL)	Time to Echo (ms)	Scan Time (min)
IT-01	1, 776	50.07	223	62	22.200
IT-02	8, 336	50.01	97	62	104.000
IT-03	2, 544	50.20	183	62	32.000
IT-04	5, 248	50.02	121	62	60.550
IT-05	1, 616	50.30	235	62	20.220
IT-06	1, 456	50.18	228	62	18.267
IT-07	3, 632	50.05	159	62	45.383
IT-08	2, 496	50.12	196	62	31.183
IT-09	8, 512	50.08	112	62	106.000
IT-10	416	50.21	421	62	5.200
IT-11	1, 552	50.16	263	62	19.433

Geomechanical Data Acquisition

The average length-to-diameter ratio of the samples was fixed at approximately 2.5, for the purpose of reducing sample geometry influence in line with the procedure stipulated by the International Society for Rock Mechanics (Ulusay & Hudson, 2007). The dry bulk density (ρ) for the samples without any moisture present were measured and recorded after drying the samples at 105 ºC for 24 hours. The UCS analysis was carried out at the Material Testing Laboratory, Faculty of Civil and Environmental Engineering, University of Lagos, Lagos, Nigeria. The universal testing machine (UTM) used consists of: (a) a servo-hydraulic frame system (DYE-2000) with a 2000 kN maximum load capacity; platens lightly lubricated for uniform distribution of load and friction reduction; (b) a strain gauge for measurement of sample deformation and dial gauge for recording platen displacement; and (c) a data acquisition system with software interface for real-time records of stress-strain data. Tests are typically performed on intact lengths of prepared cores with the maximum axial load sustained at the point of failure recorded. In this study, the increasing loads and corresponding strain were monitored simultaneously and recorded. Each test was subjected to two cycles of load and unloading within the elastic region to ensure accurate stress-strain relation. The strain gauge records the lateral deformation, as each sample was placed at the center of the static plane before compression by the plunger at a downward speed of 0.6 mm/min till crushing to avoid any dynamic effects (Ulusay, 2015).

The measured uniaxial compressional strength (σ_c) is the highest compressive stress a sample can withstand in one direction without any lateral confinement. This parameter determines the presence of cracks, fractures or crumbles under the influence of a load. It is mathematically derived as:

$$\sigma_c = \frac{L}{A} \quad (9)$$

L is the maximum load (N) on the sample at failure; A is the sample cross-sectional area of the sample (m^2).

The elastic modulus (E) is the quantitative determination of rock's stiffness; which is usually greatly affected by the microstructure of the rock. Mathematically, elastic modulus is the proportion of stress (σ) to strain (ε) as given below:

$$E = \frac{\sigma}{\varepsilon} \quad (10)$$

In this work, the elastic modulus was estimated from the slope of the linear portion of the stress-strain curve.

The modulus ratio (M_R) is the proportion of elastic modulus to uniaxial compressive strength of the samples. It was estimated using the expression:

$$M_R = \frac{E}{\sigma_c} \quad (11)$$

M_R is a dimensionless parameter that predict the brittleness and deformability of the iron ore samples. All these parameters were analysed via crossplots using MATLAB software.

RESULTS AND DISCUSSION

XRF Analysis

The major oxides compositions of the studied samples are haematite (Fe_2O_3), silica (SiO_2) and alumina (Al_2O_3) in the ranges of 52.01 – 54.25%, 20.84 – 22.50% and 11.61 – 13.12%, respectively (Figure 5). The mean proportion by weight of iron (Fe) contents in the samples was computed as 37.2%. These values imply that the studied Itakpe iron ores are low-grade ores which would require substantial processing and enrichment through beneficiation for economic viability. In commercial iron ores, acceptable purity limits are generally less than 6% for SiO_2 and less than 4% for Al_2O_3 in the raw ore to prevent adverse effect in the iron production process (Muwanguzi et al., 2012a; Sun et al., 2023).

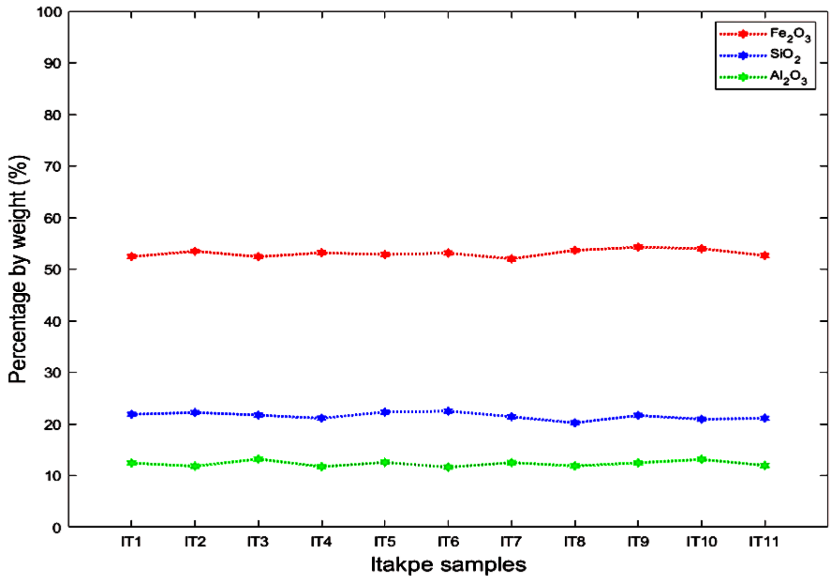

Figure 5: Percentage by weight of oxides composition for the IT- samples

NMR Analysis

Pore Morphology

Figure 6 presents the NMR-T_2 spectra for all the eleven IT-samples. Generally, the spectra show a fairly connected pores with bimodal T_2-distribution as the dominant type except for sample IT-11 which shows distinct unimodal distribution. The NMR-T_2 spectra manifest some peaks: P_1 for the micropores with short transverse relaxation times (T_2 < 10 ms) and P_2 for the mesopores with intermediate relaxation times (10 ms < T_2 < 100 ms) (Yao et al., 2010a, 2010b, 2015; Olatinsu et al., 2017; Li et al., 2020, 2022; Ige-Adeyeye et al., 2026). Furthermore, the narrow continuous path linking the pore types revealed in the NMR-T_2 spectra is an indication of the samples' low effective porosity, suggesting their susceptibility to breakage (Li et al., 2017). The IT-samples with similar NMR-T_2 spectra distribution and pore morphology were grouped for further detailed description.

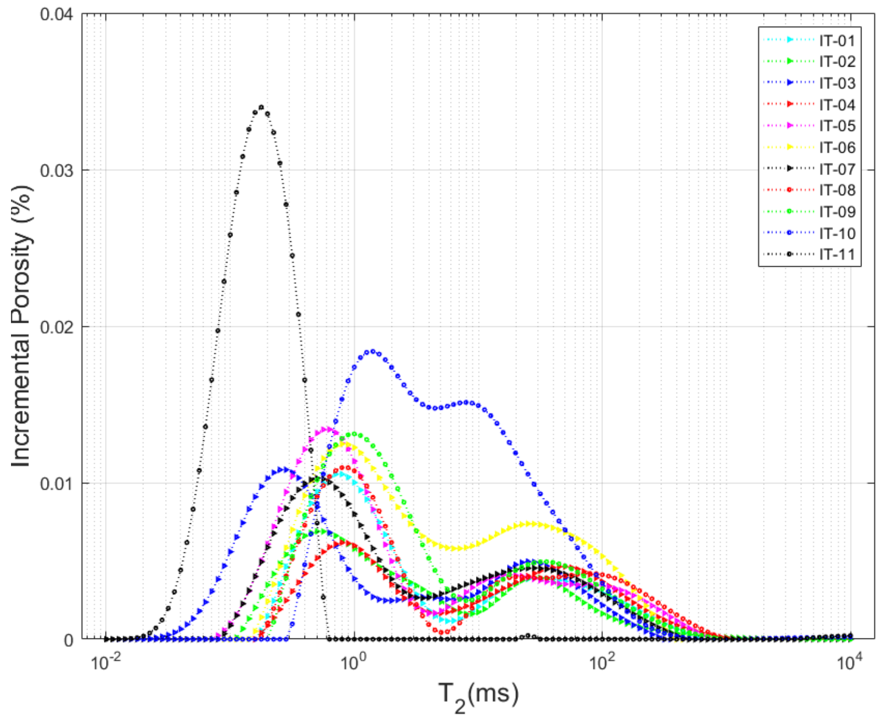

Figure 6: The NMR-T_2 spectra of Itakpe iron ore samples showing the pore distribution and connectivity

Figure 7 presents the NMR-T_2 spectra of IT-01, IT-02, IT-04, IT-07 and IT-09 which show similar pore morphology. The NMR-T_2 spectra are bimodal and reveal fairly connected pores with only two peaks (P_1 and P_2) as shown for each sample in Figure 8. The corresponding transverse relaxation time of these samples are in the ranges, 0.5012 – 1.0 ms for the micropores and 28.18 – 44.67 ms for the mesopores, respectively. IT-11 reflects an anomalous micropore volume, with a peak corresponding to 0.1778 ms.

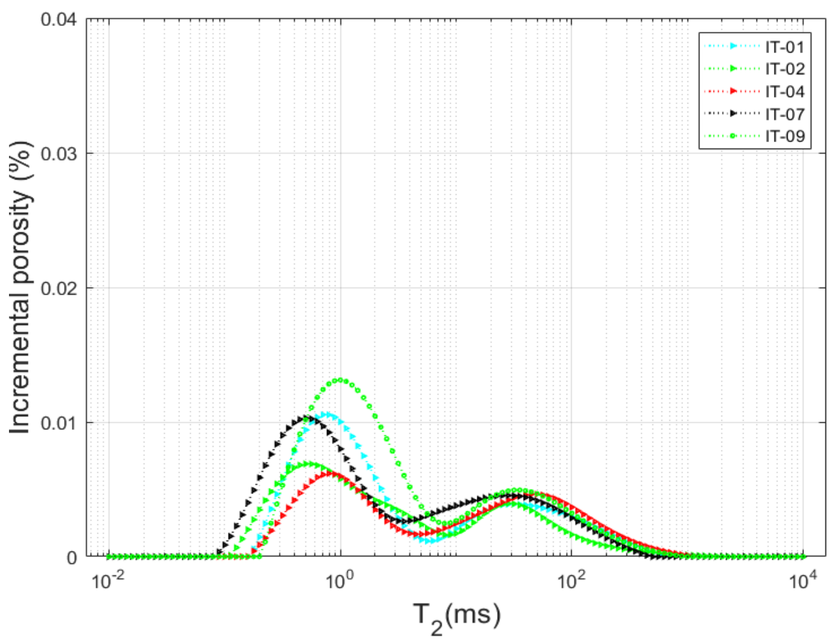

Figure 7: Grouped NMR-T_2 spectrum of IT-01, IT-02, IT-04, IT-07 and IT-09

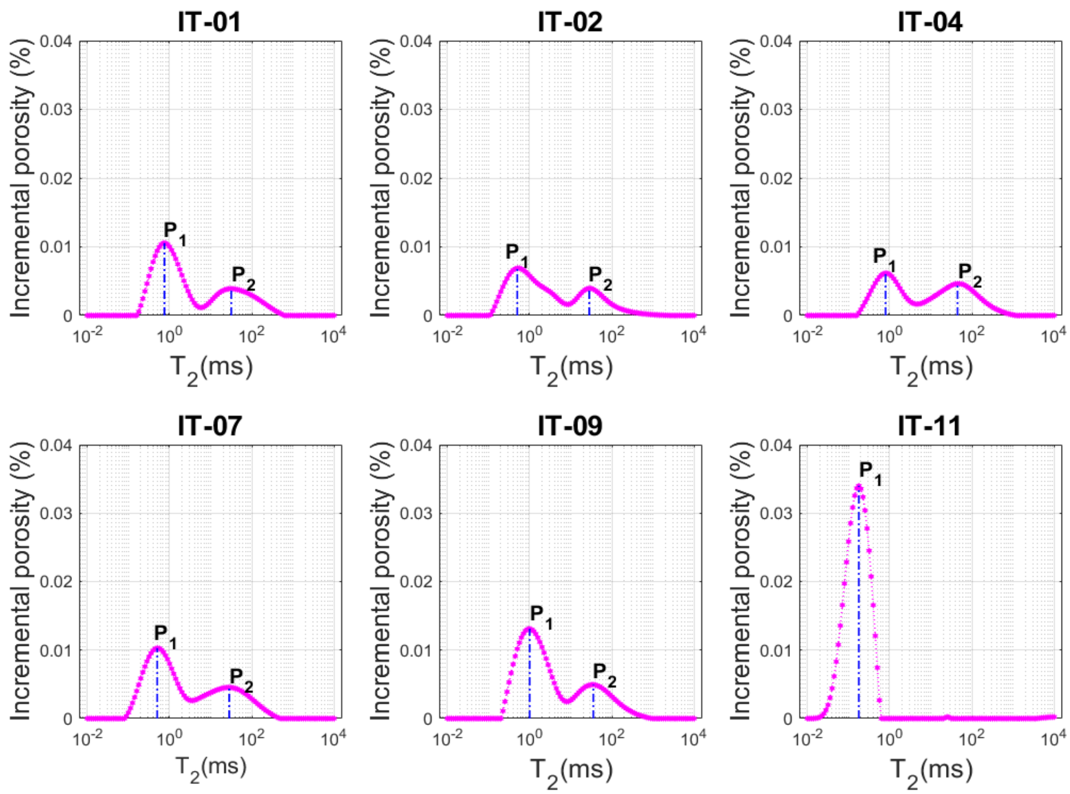

Figure 8: NMR-T_2 spectrum of IT-01, IT-02, IT-04, IT-07, IT-09 and IT-11

Figure 9 shows the combined NMR-T_2 spectra of samples IT-05 and IT-08 with matching pore configurations. The NMR-T_2 spectra of this group is typically bimodal (peaks P_1 and P_2), but with poor connectivity between the micropores and mesopores. P_2 further manifest low subpeaks P_{2a}, P_{2b} in the mesopore region as shown in Figure 10. The corresponding transverse relaxation time of these peaks has ranges 0.631 – 0.7943 ms for the micropores and 17.78 – 79.43 ms for the mesopores, respectively. The observed subset of double peaks P_{2a} and P_{2b} in the mesopore regions, are likely two distinct pores which are not fully developed.

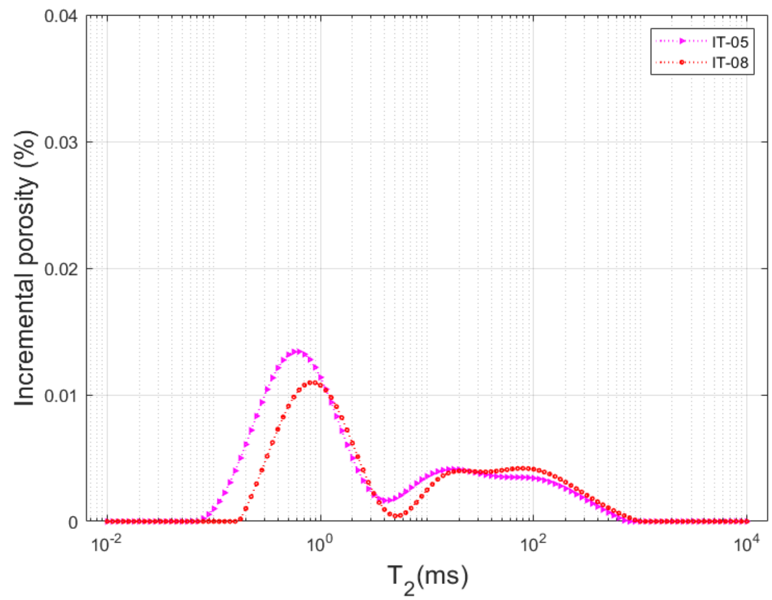

Figure 9: NMR-T_2 spectrum of IT-05 and IT-08

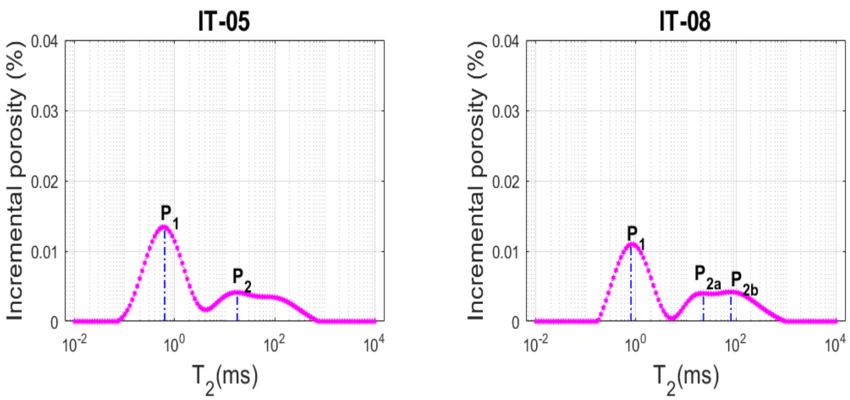

Figure 10: NMR-T_2 spectrum of IT-05 and IT-08

Figure 11 shows the combined NMR-T_2 spectra of samples IT-03, IT-06 and IT-10. The NMR-T_2 spectra of this group is also bimodal and with well-connected micropores and mesopores. The pore volume of IT-10 shows two subpeaks (P_{1a} and P_{1b}) within the micropore region, while IT-03 and IT-06 manifest two recognisable peaks, P1 for the micropores and P2 for the mesopores (Figure 12). The corresponding transverse relaxation time of these peaks ranges are 0.2818 – 1.413 ms (micropores) and 7.943 – 25.12 ms (mesopores), respectively.

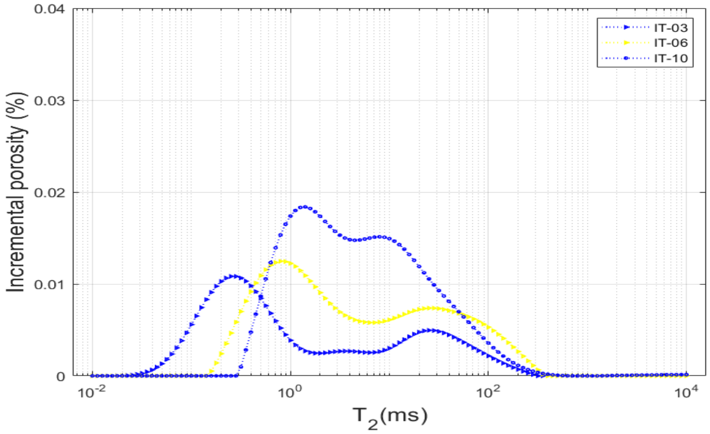

Figure 11: NMR-T_2 spectrum of IT-03, IT-06 and IT-10

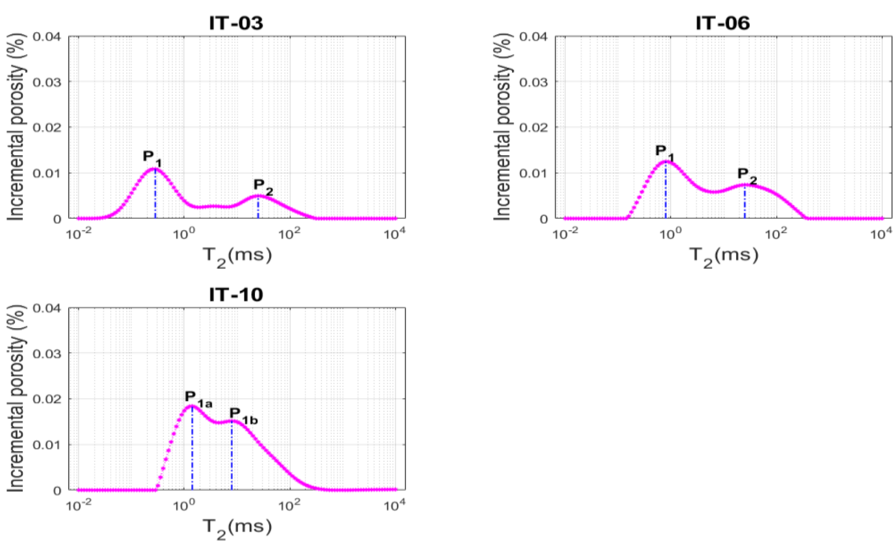

Figure 12: The NMR-T_2 spectrum of IT-03, IT-06 and IT-10

Total Porosity

Table 2 presents the computed total porosity for the samples obtained from WIP and NMR techniques for comparison. The crossplot of NMR versus WIP (Figure 13) gives a linear regression model and is represented by equation (12).

$$\phi_{NMR} = 0.30989\phi_{WIP} + 0.21387 \quad (12)$$

where ϕ_{NMR} is the NMR porosity and ϕ_{WIP} is the porosity by WIP.

The coefficient of correlation and root mean square (RMS) values are 0.87496 and 0.03115, respectively. The average porosity value for NMR and WIP techniques across all the samples are 0.365p.u. and 0.488 p.u., respectively. The relationship shows 87% correlation despite the unusual value for IT-11. The good correlation attests to the high degree of accuracy of NMR measurements and its interpretation.

Table 2: Results of porosity, water content and pore volume from NMR and WIP techniques

Samples	Porosity by NMR (%)	Porosity by WIP (%)	NMR Water Content (mL)	Pore Volume by WIP (cc)
IT-01	0.2811	0.3901	0.2226	0.309
IT-02	0.2324	0.2151	0.0973	0.090
IT-03	0.3324	0.2736	0.1834	0.151
IT-04	0.2874	0.2721	0.1212	0.145
IT-05	0.3731	0.3581	0.1835	0.226
IT-06	0.4540	0.8069	0.2279	0.405
IT-07	0.3242	0.3848	0.1592	0.189
IT-08	0.3044	0.1844	0.1965	0.119
IT-09	0.4301	0.7083	0.1118	0.216
IT-10	0.4931	0.8240	0.3421	0.550
IT-11	0.5053	0.9552	0.2635	0.498

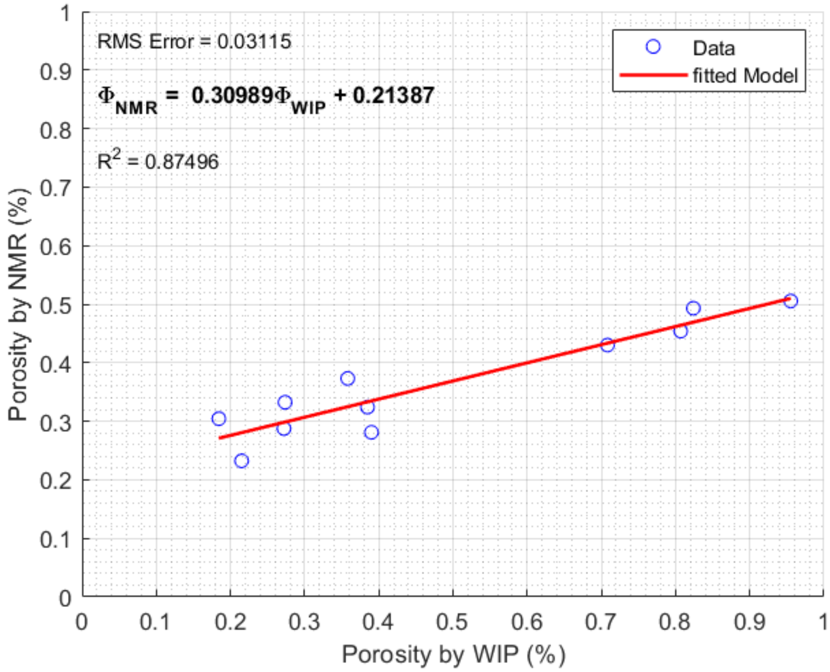

Figure 13: Crossplot of NMR porosity against WIP porosity for the IT-samples

NMR Water Content and WIP Pore Volume

The summary of NMR water content and the WIP pore volume is given in Table 2, while the crossplot of the two parameters is presented in Figure 14. The crossplot depicts a linear regression model represented by equation (13) with coefficient of correlation and RMS error value of 0.75683 and 0.033749, respectively.

$$W_{NMR} = 0.39808W_{WIP} + 0.086851 \quad (13)$$

where W_{NMR} is the NMR water content and W_{WIP} is the WIP pore water volume.

This expression indicates a 76% correlation, which is considered reasonably fair and signifies the effectiveness of NMR measurement and interpretation in characterising geological materials.

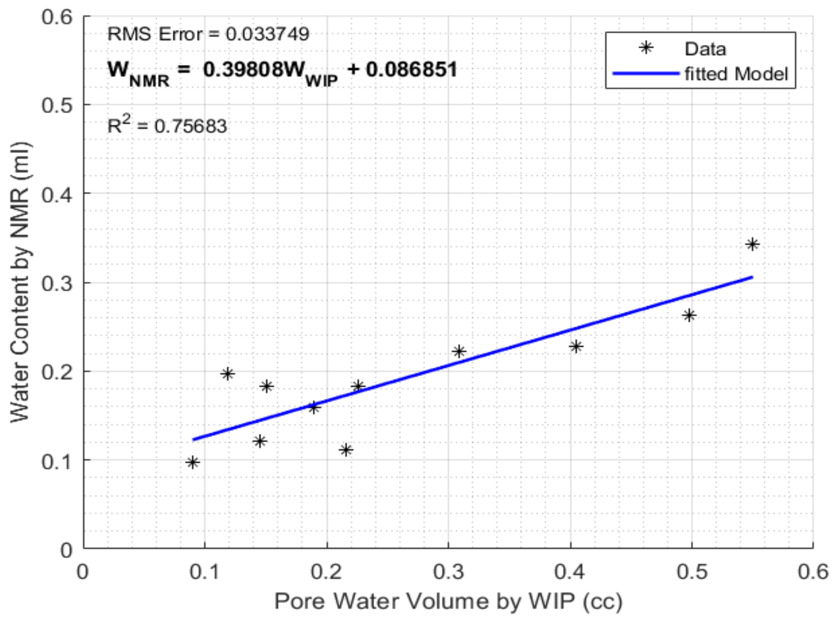

Figure 14: Crossplot of NMR water content against WIP pore volume determination

Geomechanical Analysis

Uniaxial Compressive Strength

Table 3 presents the measured uniaxial compressive strength (σ_c) and dry bulk density (ρ) for each of the investigated IT-samples. σ_c has a range of 71 – 146 MPa and ρ has a range of 3.24 – 3.72 g/cm^3 with average values of 101.28 MPa and 3.46 g/cm^3, respectively. Thus, the studied iron ore samples can be classified as high strength (>100 MPa) and high-density ores (>2.6 g/cm^3) (Nilsen & Palmström, 2000; Ulusay & Hudson, 2007). The plot of UCS versus dry bulk density shows an increasing exponential trend (Figure 15). The fitted model is given by equation (14), with coefficient of determination (R^2) and RMS error value of 0.9827 and 3.4657, respectively.

$$\sigma_c = 0.756e^{1.409\rho} \quad (14)$$

Table 3: Results of dry bulk density and uniaxial compression strength for the Itakpe iron ore samples

Samples	Dry Bulk Density (g/cm^3)	UCS Value (MPa)
IT-01	3.60	120.73
IT-02	3.72	146.46
IT-03	3.48	101.96
IT-04	3.65	122.94
IT-05	3.43	95.35
IT-06	3.22	73.15
IT-07	3.55	114.58
IT-08	3.56	115.48
IT-09	3.26	77.51
IT-10	3.31	74.57
IT-11	3.24	71.39

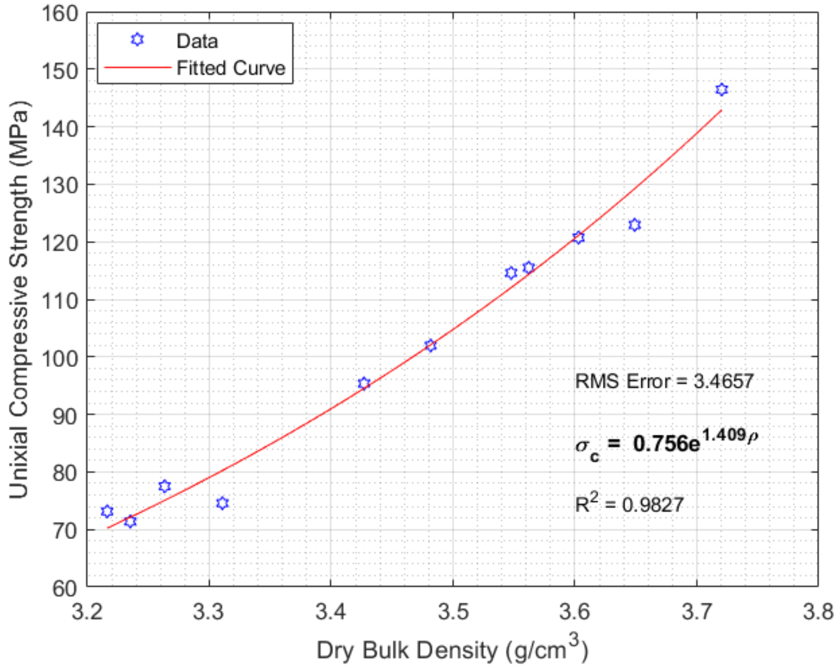

Figure 15: Crossplot of UCS against dry bulk density of IT-samples

The plot of UCS versus NMR porosity (Figure 16) shows reveals strong exponential decreasing trend as expected (Ryshkewitch, 1953; Bell & Lindsay, 1999; Chindaprasirt et al., 2009). This is an opposite trend to the plots of UCS versus dry bulk density. The fitted model is given by equation (15). The coefficient of determination and RMS error value are 0.9722 and 4.4, respectively.

$$\sigma_c = 271.4e^{-2.784\phi_{NMR}} \quad (15)$$

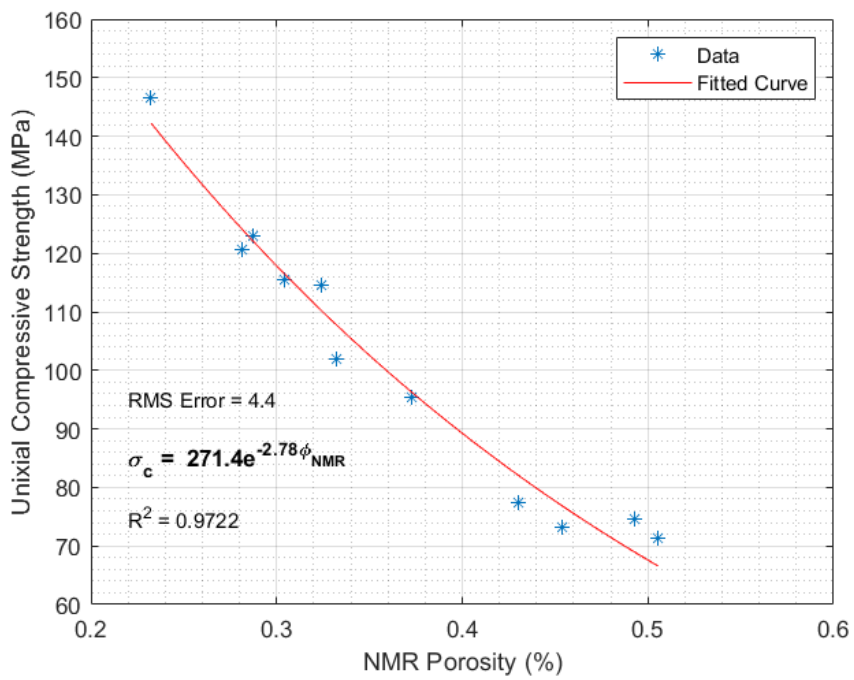

Figure 16: Crossplot of UCS against NMR porosity of IT-samples

Stress-strain Curves

Based on the previously identified three subgroups of the NMR-T_2 spectra from the pore configuration of the Itakpe samples, three crossplots arrangement of the axial stress against axial strain were established (Figures 17 – 19). The ranges of UCS values and the estimated elastic modulus are: group I (IT-01, IT-02, IT-04, IT-09 and IT-11), 71.39 – 146.46 MPa and 3.8 – 4.2 GPa, respectively; group II (IT-03, IT-06, and IT-10), 73.15 – 101.96 MPa and 95.35 – 115.48 MPa, respectively; and group II (IT-05 and IT-08), 3.5 – 4.0 GPa and 3.7 – 4.0 GPa, respectively. With the average value of the elastic modulus estimated as 3.94 GPa.

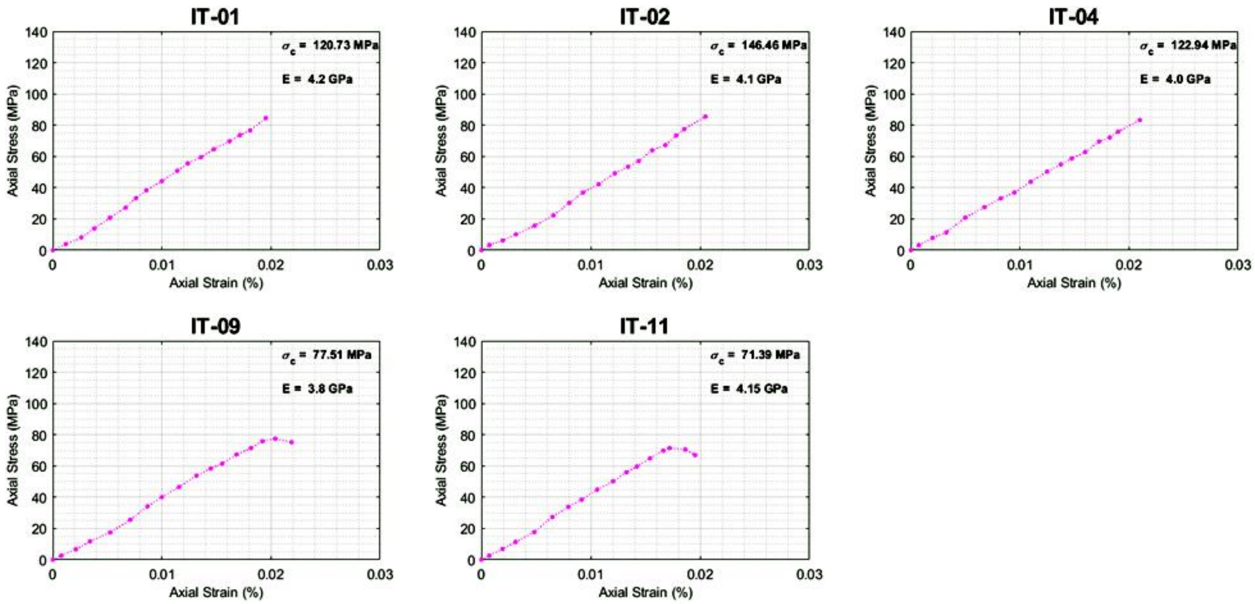

Figure 17: Crossplots of axial stress and axial strain for IT-01, IT-02, IT-04, IT-09 and IT-11

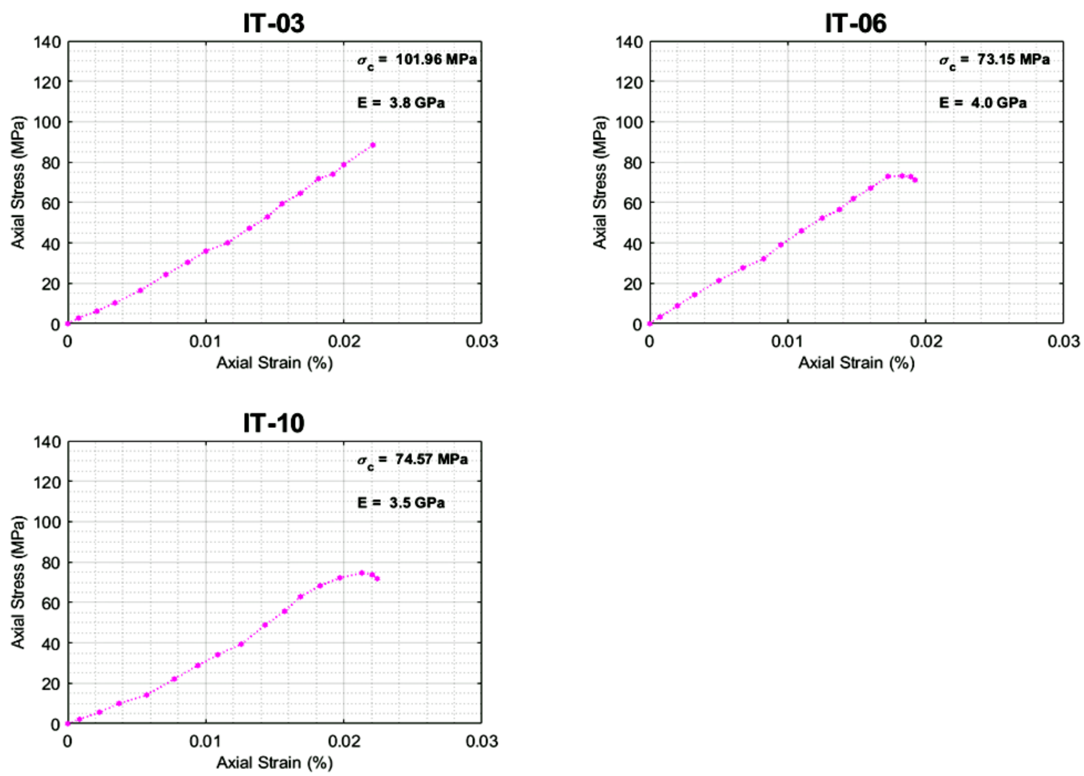

Figure 18: Crossplots of axial stress and axial strain for IT-03, IT-06 and IT-10

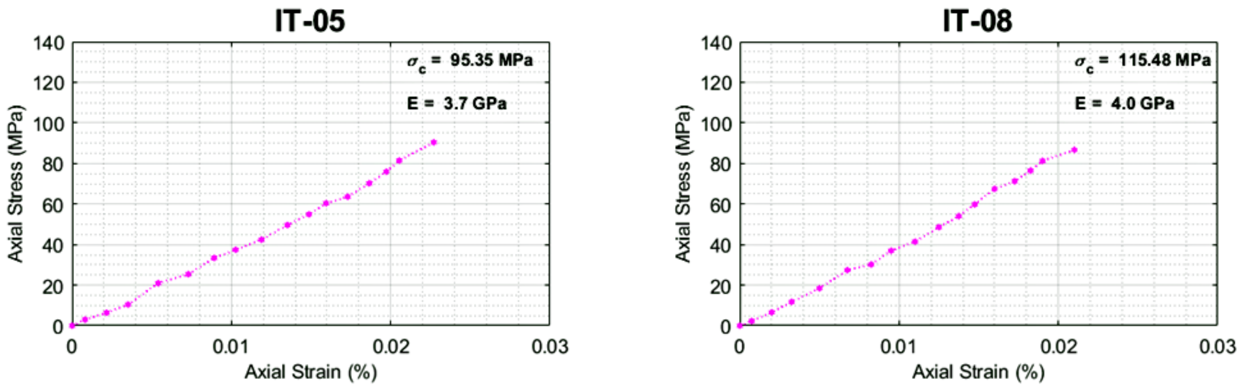

Figure 19: Crossplots of axial stress and axial strain for IT-05, and IT-08

Figure 20 shows the crossplots of elastic modulus and modulus ratio versus dry bulk density for the samples. It is observed that the elastic modulus shows no significant correlation with dry bulk density as its coefficient of determination is very small ($R^2 = 0.1535$). However, the modulus ratio shows a very strong correlation with dry bulk density in the form of an exponentially decreasing curve defined by equation (16). The R^2 and RMS error value for the modulus ratio versus bulk density are 0.9480 and 0.23373, respectively. These observations suggest a strong correlation between brittleness and density of the Itakpe iron ores.

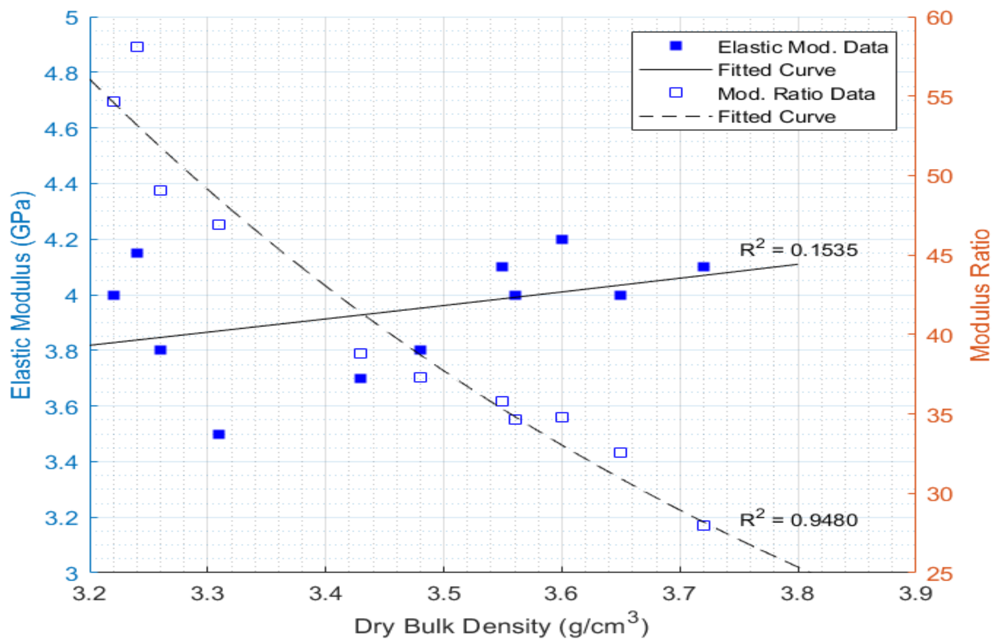

Figure 20: Crossplots of elastic modulus, modulus ratio against dry bulk density of IT-samples

$$M_R = 3858.4e^{-1.322\rho} \quad (16)$$

The plots of elastic modulus and modulus ratio versus UCS for the studied samples (Figure 21) reveal high similarity with the plots of elastic modulus and modulus ratio versus dry bulk density (Figure 20). Also, while elastic modulus shows no significant correlation with uniaxial compressive strength ($R^2 = 0.2167$), the modulus ratio (M_R) shows a very strong exponential trend with UCS, as defined by equation (17). The coefficient of determination and RMS error value are 0.9172 and 2.9504, respectively. The relationship presumably validates the strong brittle nature of Itakpe iron ores as dense and highly compacted metamorphic deposits.

$$M_R = 104.5e^{-0.009504\sigma_c} \quad (17)$$

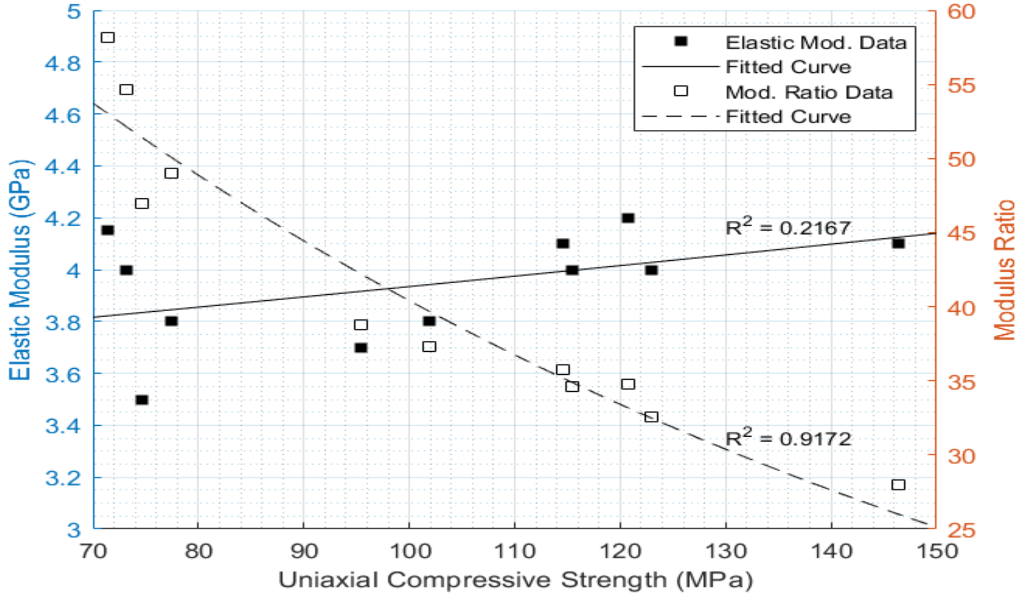

Figure 21: Crossplots of elastic modulus, modulus ratio against uniaxial compressive strength of IT-samples

The modulus ratio relationship with dry bulk density (Figure 20) and UCS (Figure 21) both reveals drop in stress after deformation for most of the IT-samples. It is presumed that the UCS might be affected by size effect than elastic modulus, however the degree depends on the heterogeneity, presence of micro-cracks and discontinuities (Hudson & Harrison, 2000). This denotes brittleness, possibly couple with internal cracks via pore structure of the rock matrix of the samples. The average UCS value of 101.28 MPa obtained for the studied Itakpe samples, is considered as high value based on ISRM (2007) classification or strong strength based on Attewell and Farmer (1976) as indicted in Table 4. This value is slightly lower than the average UCS value of 142.90 MPa for the Ajabanoko iron ore deposits which is about 4 km away from the Itakpe Hills (Adebimpe, 2013). On the global scale, this average UCS value also lie within the range of 110 – 200 MPa as seen in Table 5, for medium hardness iron cores from Australia (O'Connor et al., 2000) and is much higher than for the iron ore samples (about 67.70 MPa) from Anshan region in China (Ju et al., 2024).

Table 4: Summary of the International Society for Rock Mechanics (ISRM, 2007) standard terminology and Attewell and Farmer (1976) for UCS.

ISRM (2007)		Attewell and Farmer (1976)		
UCS Values (MPa)	**Strength Classification**	**UCS Values (MPa)**	**Strength classification**	**Typical Rock Types**
< 5	very low	10 – 20	Very weak	Weathered and weakly compacted sedimentary rocks.
5 – 25	low	20 – 40	Weak	Weakly cemented sedimentary rocks, schist
25 – 50	moderate	40 – 80	Medium	Competent sedimentary rocks; some low-density coarse-igneous rocks.
50 – 100	Medium	80 – 160	Strong	Competent igneous rocks; some metamorphic and fine-grained sandstones.
100 – 250	High			
> 250	very high			

Table 5: UCS range for Australian iron ores for comparison from O'Connor et al. (2000)

UCS values (MPa)	Ore Type
20 – 35	Friable hardness iron ore
110 – 200	Medium hardness iron ore
200 – 500	Hard iron ore

Discussion

Preliminary geochemical evaluation of iron ore is critical for determining the economic viability, planning cost-effective mining and processing strategies. Iron ore classification into different grades is based on its total iron (Fe) weight percentage. This study shows that the studied Itakpe iron ores consist of haematite (Fe_2O_3) content having the range 52.01 – 54.25% and 37% as the average weight of Fe content. Hence, the iron content of these samples is far below the high-grade benchmark of 60 – 65%. Therefore, significant beneficiation (processing) is necessary for the economic viability of the raw materials. In addition, the ores contain high level of impurities: silica (SiO_2) and alumina (Al_2O_3) in the ranges of 20.84 – 22.50% and 11.61 – 13.12%, respectively. However, for suitability as commercial iron ores, acceptable purity limits is expected to be less than 6% for SiO_2 and less than 4% for Al_2O_3.

The integrated porosity and geomechanical datasets obtained for the Itakpe banded iron ore has provided valuable information on the possible effects of pore-scale characteristics on their bulk mechanical behaviour. Porosity of iron ore is important in ore breakage consideration as an integral part of the comminution process. It also has implications in the production stage because it dictates the infiltration and penetration of reducing gas into the interior of lump ores. A high porosity of materials enhances reducibility by providing a large interfacial area for a gas-solid contact. The bimodal NMR-T_2 spectra, characterised by micropores and mesopores with moderate connectivity, reveal a pore morphology which establishes the metasedimentary origin of the Itakpe iron ore deposits. The absence of macropores in all the samples is an indication of a compact, recrystallized fabric formed through metamorphism. This interpretation is consistent with the earlier descriptions of the Itakpe deposit as a metamorphosed sedimentary iron formation. In addition, the relative volume of pore types and their connectivity directly relates to the breakage efficiency. Therefore, the presence of higher proportion of micropores compared with mesopores, couple with the complete absence of macropores, indicates significant resistance to ore breakage due to lack of "weak zones" needed to crack initial and propagation. This dominant manifestation of micropores is very common in shale and clayey materials (Olatinsu et al., 2017). In situations where the bigger pores, especially macropores or microcracks, are more prominent, resistance to ore breakage is expected to be low. This observed pore characteristics and configurations are highly relevant for mechanical response since micropores and mesopores are known to exert strong control on crack initiation and propagation because stress concentrations preferentially accumulate at grain-boundary and intra-granular voids (Tan et al., 2026). Hence, the probability of occurrence of brittle failure is high. The porosity values obtained for the Itakpe ore samples despite having high amounts of gangue (SiO_2 and Al_2O_3) and low Fe content are quite higher than the porosity values of the commercial lump iron ores used in the blast furnace (e.g., 5.9% for MBR Brazil iron ore) (Cores et al., 2007) and in the direct reduction processes (e.g., 1.2 – 5.2% for Orissa India iron ores) (Kumar et al., 2008).

Uniaxial compressive strength (UCS) values are very relevant to iron ore crusher design and rock geomechanics in mining. UCS for most iron ores varies between low to medium, with BIF and hard haematite ores in the high to very high range. There is clear contrast between the plots of UCS versus dry bulk density and UCS versus NMR porosity. While UCS versus dry bulk density shows a strong exponential increase, UCS versus NMR porosity, depicts a strong exponential decreasing trend as expected (Bell & Lindsay, 1999). The strong mechanical strength of the Itakpe iron ores may be attributed to their relatively moderate porosity and relatively uniform microstructure and pore configuration (Muwanguzi et al., 2012b).

CONCLUSION

Geochemical analysis using XRF spectroscopy; pore structure and porosity characterisation using low-field NMR/WIP techniques; and geomechanical characterisation via UCS and bulk density measurements were carried out on banded iron ore samples from Itakpe, North Central Nigeria. XRF spectroscopy reveals that the studied ore samples are low-grade with 37% iron (Fe) content by weight. The study also shows that the NMR-T_2 spectra are typically bimodal and consist of micropore with T_2 in the range, 0.2818 – 1.413 ms and mesopores with T_2 in the range, 7.943 – 79.43 ms. The pore structure exhibits moderate connectivity and no indication of macropores. The revealed pore characteristics are highly relevant for iron ore mechanical responses. The computed average porosity values from NMR and WIP techniques are 0.365 p.u. and 0.488 p.u., respectively. High correlations between porosity and water content evaluated from NMR and WIP methods were obtained as 87% and 76%, respectively. Hence, this validates the accuracy of NMR methodology in solid mineral characterisation. The computed average UCS, elastic modulus and dry bulk density of the studied samples are 101.28 MPa, 3.94 GPa and 3.46 g/cm^3, respectively. The coefficients of determination for UCS versus dry bulk density, UCS versus NMR porosity, modulus ratio versus dry bulk density and modulus ratio versus UCS, were found as 98%, 97%, 98% and 92%, respectively. However, no significant correlation was observed between elastic modulus and dry bulk density as well as between elastic modulus and UCS. These findings establish that the porosity of the Itakpe iron ores can be evaluated using low-field NMR, in connection with established relationships for UCS. The exponential curves obtained for UCS versus bulk density (increasing trend) and UCS versus NMR porosity (decreasing trend) are in agreement with previous works in rock mechanics. The fairly homogeneous microstructure, pore morphology, and comparatively moderate porosity of the Itakpe iron ores may be responsible for their high mechanical strength. Thus, these good physical characteristics will enhance mining stability, safety, efficient drilling and blasting. Therefore, the integration of NMR and geomechanical techniques can reliably: (i) predict mechanical behaviour without destructive testing; (ii) complement traditional porosity methods; and (iii) assist in mine design for safety and assist in ore optimisation. The outcomes of this study have implications for other local BIF deposits in Nigeria and other similar geological environments globally.

REFERENCES

Adebimpe, R.A., 2013. Mine Equipment Selection for Ajabanoko Iron Ore Deposit, Kogi State, Nigeria. *Science Research*, 1, 25. https://doi.org/10.11648/j.sr.20130102.13.

Adedeji, F.A. and Sale, F.R., 1984. Characterization and reducibility of Itakpe and Agbaja (Nigerian) iron ores. Clay miner. 19, 843 – 856. https://doi.org/10.1180/claymin.1984.019.5.12

Adejuwon, B., Ibeneme Sabinus, I., Osizemete, A., Obioha Young, E., Abba, A., 2020. Quality Assessment and Reserve Estimation of the Egnaeja Iron Ore Deposit, North Central Nigeria using Integrated Approach. International Journal of Earth Science and Geophysics, 6, 2. https://doi.org/10.35840/2631-5033/1837.

Afeni, T.B., Lawal, A.I., Adeyemi, R.A., 2020. Re-examination of Itakpe iron ore deposit for reserve estimation using geostatistics and artificial neural network techniques. Arab J Geosci 13, 657. https://doi.org/10.1007/s12517-020-05644-9.

Akande, S., Ajaka, E.O., Alabi, O.O., Olatunji, T.A., 2020. Effects of varied process parameters on froth flotation efficiency: A case study of Itakpe iron ore. Nig. J. Tech. 39, 807 – 815. https://doi.org/10.4314/njt.v39i3.21.

Akinrinsola, A.O., Adekeye, J.I.D., 1993. A geostatistical ore reserve estimation of the Itakpe iron ore deposits, Okene, Kogi State. Journ. Mining. And Geology 29, 19–25.

Alabi, O. O., Sedara, S. O., Olatona, G. I., Olaleye, A. O., & Kasali, A. A. (2025). Mineral Resource Exploration Potential in the Ado-Ekiti-Ilesa Region of Southwest, Nigeria using Aeromagnetic Survey. *Nigerian Journal of Physics*, 34(3), 43-52.

Ameh, E.G., 2014. Geochemical distribution of heavy metals in soil around Itakpe iron-ore mining area-a statistical approach. Research journal of environmental and earth sciences 6, 118–126.

Amigun, J.O., Ako, B.D., 2009. Rock density-A tool for mineral prospection: A case study of Ajabanoko iron ore deposit, Okene SW Nigeria. The pacific journal of science and technology 10, 733–741.

Annor, A.E., Freeth, S.J., 1985. Thermo-tectonic evolution of the basement complex around Okene, Nigeria, with special reference to deformation mechanism. Precambrian Research 28, 269–281.

Anovitz, L.M., Cole, D.R., 2015. Characterization and Analysis of Porosity and Pore Structures. Reviews in Mineralogy and Geochemistry 80, 61–164. https://doi.org/10.2138/rmg.2015.80.04.

Anudu, G.K., Stephenson, R.A., Macdonald, D.I.M., 2014. Using high-resolution aeromagnetic data to recognise and map intra-sedimentary volcanic rocks and geological structures across the Cretaceous middle Benue Trough, Nigeria. Journal of African Earth Sciences 99, 625–636. https://doi.org/10.1016/j.jafrearsci.2014.02.017.

Armstrong, P., Knieke, C., Mackovic, M., Frank, G., Hartmaier, A., Göken, M., Peukert, W., 2009. Microstructural evolution during deformation of tin dioxide nanoparticles in a comminution process. Acta Materialia 57, 3060 – 3071. https://doi.org/10.1016/j.actamat.2009.02.049.

Atapour, H., Mortazavi, A., 2018a. The effect of grain size and cement content on index properties of weakly solidified artificial sandstones. J. Geophys. Eng. 15, 613 – 619. https://doi.org/10.1088/1742-2140/aaa14a

Atapour, H., Mortazavi, A., 2018b. The influence of mean grain size on unconfined compressive strength of weakly consolidated reservoir sandstones. Journal of Petroleum Science and Engineering 171, 63–70. https://doi.org/10.1016/j.petrol.2018.07.029

Attewell, P.B. and Farmer, I.W. (1976) Principles of Engineering Geology. Chapman and Hall, London. https://doi.org/10.1007/978-94-009-5707-7.

Bell, F.G. and Lindsay, P. 1999. The petrographic and geomechanical properties of some sandstones from the

Newspaper Member of the Natal Group near Durban, South Africa. Eng. Geol. 53, 57-81.

Bello, R., Onifade, Y.S., 2016. Discrimination of reservoir fluid contacts using compressional and shear wave velocity. Glo Jnl Pure Appl Sci 22, 177. https://doi.org/10.4314/gjpas.v22i2.7

Benavides, F., Leiderman, R., Souza, A., Carneiro, G., Bagueira De Vasconcellos Azeredo, R., 2020. Pore size distribution from NMR and image-based methods: A comparative study. Journal of Petroleum Science and Engineering 184, 106321. https://doi.org/10.1016/j.petrol.2019.106321

Bett, A. K. and Maranga, S. M. (2012). Considerations for Beneficiation of Low-Grade Iron Ore for Steel Making in Kenya. Proceedings of the 2012 Mechanical Engineering Conference on Sustainable Research and Innovation, Volume 4, 3rd-4th May 2012.

Beukes, N. J., Gutzmer, J., & Mukhopadhyay, J. (2003). The geology and genesis of high-grade hematite iron ore deposits. Applied Earth Science, 112(1), 18–25. https://doi.org/10.1179/037174503225011243.

Bevilacqua, P., Ferrara, G., 1996. Comminution of porous materials. International Journal of Mineral Processing 44–45, 117–131. https://doi.org/10.1016/0301-7516(95)00023-2

Blümich, B., 2019. Low-field and benchtop NMR. Journal of Magnetic Resonance 306, 27–35. https://doi.org/10.1016/j.jmr.2019.07.030

Blümich, B., Casanova, F., Appelt, S., 2009. NMR at low magnetic fields. Chemical Physics Letters 477, 231–240. https://doi.org/10.1016/j.cplett.2009.06.096

Bradshaw, D., 2014. The role of process mineralogy in improving the process performance of complex sulphide ores, in: Proceedings of the XXVII International Mineral Processing Congress. pp. 1–23.

Carr, H.Y., Purcell, E.M., 1954. Effects of diffusion on free precession in nuclear magnetic resonance experiments. Phys. Rev. 94, 630–638. https://doi.org/10.1103/PhysRev.94.630

Casieri, C., De Luca, F., Nodari, L., Russo, U., Terenzi, C., 2010. Detection of magnetic environments in porous media by low-field 2D NMR relaxometry. Chemical Physics Letters 496, 223–226.

Chatterjee, R. and Mukhopadhyay, M. 2002. Petrophysical and geomechanical properties of rocks from the oilfields of the Krishna-Godavari and Cauvery Basins, India. Bull. Eng. Geol. Environ. 2002, 61, 169–178.

Chindaprasirt, P., Hatanaka, S., Mishima, N., Yuasa, Y. and Chareerat, T., 2009. Effects of binder strength and aggregate size on the compressive strength and void ratio of porous concrete. *International journal of minerals, metallurgy and materials*, *16*(6), pp.714-719.

Clout, J.M.F. and Manuel, J.R. (2015). Mineralogical, chemical, and physical characteristics of iron ore. Editor(s): Liming Lu, Iron Ore, Woodhead Publishing, 45-84. https://doi.org/10.1016/B978-1-78242-156-6.00002-2.

Coates, G.R., Xiao, L., Prammer, M.G., 1999. NMR logging: Principles and Interpretation. Halliburton Energy Service, Huston, Texas.

Connolly, P.R.J., Yan, W., Zhang, D., Mahmoud, M., Verrall, M., Lebedev, M., Iglauer, S., Metaxas, P.J., May, E.F., Johns, M.L., 2019. Simulation and experimental measurements of internal magnetic field gradients and NMR transverse relaxation times (T2) in sandstone rocks. Journal of Petroleum Science and Engineering 175, 985–997. https://doi.org/10.1016/j.petrol.2019.01.036

Cores, A., Babich, A., Muñiz, M., Isidro, A., Ferreira, S. and Martin, R. 2007. Iron ores, fluxes and tuyere injected coals used in the blast furnace. Ironmaking and Steelmaking, 34(3), 231-240.

Dalirnasab, A., Marji, M.F., Nejati, H.-R., Mohebi, M., 2024. Effects of porosity on the strength and mechanical behaviour of porous geo-materials under cyclic loading. *Rudarsko-geološko-naftni zbornik* 39, 15–30. https://doi.org/10.17794/rgn.2024.2.2

Downey, K., Bermel, W., Soong, R., Lysak, D.H., Ronda, K., Steiner, K., Costa, P.M., Wolff, W.W., Decker, V., Busse, F., Goerling, B., Haber, A., Simpson, M.J., Simpson, A.J., 2024. Low-field, not low quality: 1D simplification, selective detection, and heteronuclear 2D experiments for improving low-field NMR spectroscopy of environmental and biological samples. Magnetic Reson in Chemistry 62, 345–360. https://doi.org/10.1002/mrc.5401

Dunn, K.-J., Bergman, D.J., LaTorraca, G.A., 2002. Nuclear magnetic resonance: Petrophysical and logging applications. Elsevier.

Fadare, V.O., 1983. Iron Ore Formation—The Okene-Ajaokuta-Lokoja Areas of Kogi State. A Potential Supply

Base for Steel Plant at Ajaokuta. Journal of Mining and Geology 20, 209–214.

Faruwa, A.R., Qian, W., Akinsunmade, A., Akingboye, A.S., Dusabemariya, C., 2021. Aeromagnetic and remote sensing characterization of structural elements influencing iron ore deposits and other mineralization in Kabba, southwestern Nigeria. Advances in Space Research 68, 3302–3313. https://doi.org/10.1016/j.asr.2021.06.024

Feng, S., Xu, Z., Chai, J., Li, Y., 2020. Using pore size distribution and porosity to estimate particle size distribution by nuclear magnetic resonance. Soils and Foundations 60, 1011–1019. https://doi.org/10.1016/j.sandf.2020.05.006

Gareev, K.G. (2023). Diversity of Iron Oxides: Mechanisms of Formation, Physical Properties and Applications. Magnetochemistry 2023, 9(5), 119; https://doi.org/10.3390/magnetochemistry9050119.

Gholami, R., Fakhari, N., 2017. Support Vector Machine: Principles, Parameters, and Applications, in: Handbook of Neural Computation. Elsevier, pp. 515–535. https://doi.org/10.1016/B978-0-12-811318-9.00027-2

Golsanami, N., Zhang, X., Yan, W., Yu, L., Dong, H., Dong, X., Cui, L., Jayasuriya, M.N., Fernando, S.G., Barzgar, E., 2021. NMR-Based Study of the Pore Types' Contribution to the Elastic Response of the Reservoir Rock. Energies 14, 1513. https://doi.org/10.3390/en14051513

Grunewald, E., Knight, R., 2011. A laboratory study of NMR relaxation times in unconsolidated heterogeneous sediments. *Geophysics* 76, G73–G83. https://doi.org/10.1190/1.3581094.

Han, D. Zhu, J. And Leung, Y. 2022. Failure strength and fracture characteristics of rock with discontinuity under indirect tension. Journal of Rock Mechanics and Geotechnical Engineering, 14(6), 1810-1822. https://doi.org/10.1016/j.jrmge.2022.02.007.

Holmes, R.J. 2013. Overview of the Australian iron ore industry. In: Rankin, W.J. (Ed.), Australian Mining and Metallurgical Operating Practices. The Australian Institute ofMining and Metallurgy: Melbourne, Australia, 1379-1384.

Holmes, R.J. and Lu, L. (2015). Introduction: Overview of the global iron ore industry. Iron Ore, 42p. http://dx.doi.org/10.1016/B978-1-78242-156-6.00001-0. Elsevier Ltd.

Holmes, R.J., Lu, Y. and Lu, L. (2022). Chapter 1 - Introduction: Overview of the global iron ore industry, Editor(s): Liming Lu, In Woodhead Publishing Series in Metals and Surface Engineering, Iron Ore (Second Edition), Woodhead Publishing, 1-56. https://doi.org/10.1016/B978-0-12-820226-5.00023-9.

Ifediegwu, S.I., Nnebedum, D.O., Nwatarali, A.N., 2019. Identification of groundwater potential zones in the hard and soft rock terrains of Kogi State, North Central Nigeria: an integrated GIS and remote sensing techniques. SN Appl. Sci. 1, 1151. https://doi.org/10.1007/s42452-019-1181-1

Ige-Adeyeye, A.A., Olatinsu, O.B., Ozebo, V.C., Esteban, L., 2026. Pore size characterization of Cretaceous ironstone by low-field nuclear magnetic resonance technique. Geosystems and Geoenvironment 5, 100449. https://doi.org/10.1016/j.geogeo.2025.100449

Isah, S. and Aliyu, B. (2024). Unveiling the Mineral Wealth of Kogi State, Nigeria: A Comprehensive Inventory and Assessment. Earth Sciences, 13(6), 246-281. https://doi.org/10.11648/j.earth.20241306.12.

ISRM (2007) The complete ISRM Suggested Methods for rock characterization, testing and monitoring: 1974–2006. In: Ulusay R, Hudson JA (eds) Suggested Methods prepared by the Commission on Testing Methods, International Society for Rock Mechanics, compilation arranged by the ISRM Turkish National Group, Kozan Ofset, Ankara, Turkey.

Iwasaki, I., Prasad, M.S., 1989. Processing Techniques for Difficult-to-treat Ores by Combining Chemical Metallurgy and Mineral Processing. Mineral Processing and Extractive Metallurgy Review 4, 241–276. https://doi.org/10.1080/08827508908952639

Jégourel, Y., 2020. The global iron ore market: From cyclical developments to potential structural changes. The Extractive Industries and Society 7, 1128–1134. https://doi.org/10.1016/j.exis.2020.05.015

Jeng, F.S., Weng, M.C., Lin, M.L., Huang, T.H., 2004. Influence of petrographic parameters on geotechnical properties of tertiary sandstones from Taiwan. Engineering Geology 73, 71–91. https://doi.org/10.1016/j.enggeo.2003.12.001

Jin, S., Zhou, J., Zhao, X., Sun, L., 2021. Quantitative relationship between pore size distribution and compressive strength of cementitious materials. Construction and Building Materials 273, 121727. https://doi.org/10.1016/j.conbuildmat.2020.121727

Ju, Y., Jin, A., Zhao, Y., Tang, S., 2024. Iron ore grade's impact on uniaxial compression behavior and acoustic emission characteristics. Materials Today Communications 39, 108856. https://doi.org/10.1016/j.mtcomm.2024.108856.

Keating, K., Knight, R., 2007. A laboratory study to determine the effect of iron oxides on proton NMR measurements. *Geophysics* 72, E27–E32. https://doi.org/10.1190/1.2399445

Keating, K., Knight, R., 2010. A laboratory study of the effect of Fe(II)-bearing minerals on nuclear magnetic resonance (NMR) relaxation measurements. *Geophysics* 75, F71–F82. https://doi.org/10.1190/1.3386573

Keating, K., Knight, R., 2012. The effect of spatial variation in surface relaxivity on nuclear magnetic resonance relaxation rates. *Geophysics* 77, E365–E377. https://doi.org/10.1190/geo2011-0462.1

Kenyon, W.E., 1997. Petrophysical Principles of Applications of NMR Logging. The Log Analyst 38.

Khanlari, G.-R., Heidari, M., Sepahigero, A.-A., Fereidooni, D., 2014. Quantification of strength anisotropy of metamorphic rocks of the Hamedan province, Iran, as determined from cylindrical punch, point load and Brazilian tests. Engineering Geology 169, 80–90. https://doi.org/10.1016/j.enggeo.2013.11.014

Kholodov, V.N. and Butuzova, G.Y. (2008). Siderite formation and evolution of sedimentary iron ore deposition in the Earth's history. Geol. Ore Deposits 50, 299–319 (2008). https://doi.org/10.1134/S107570150804003X.

King, R.P., 1994. Comminution and liberation of minerals. Minerals Engineering 7, 129–140. https://doi.org/10.1016/0892-6875(94)90059-0

Klein, B., Wang, C., Nadolski, S., 2018. Energy-efficient comminution: best practices and future research needs, in: Awuah-Offei, K. (Ed.), Energy Efficiency in the Minerals Industry, Green Energy and Technology. Springer International Publishing, Cham, pp. 197–211. https://doi.org/10.1007/978-3-319-54199-0_11

Kleinberg, R.L., 1996. Utility of NMR T2 distributions, connection with capillary pressure, clay effect, and determination of the surface relaxivity parameter ρ2. Magnetic resonance imaging 14, 761–767.

Kleinberg, R.L., 2001. NMR measurement of petrophysical properties. Concepts in Magnetic Resonance 13, 404–406.

Kleinberg, R.L., Farooqui, S.A., Horsfield, M.A., 1993. T1/T2 ratio and frequency dependence of NMR relaxation in porous sedimentary rocks. Journal of Colloid and Interface Science 158, 195–198.

Kleinberg, R.L., Horsfield, M.A., 1990. Transverse relaxation processes in porous sedimentary rock. Journal of Magnetic Resonance (1969) 88, 9–19. https://doi.org/10.1016/0022-2364(90)90104-H

Korbel, C., Foucaud, Y., Vanderbruggen, A., 2026. Mineral processing applied to the treatment of primary and secondary ores, in: Sustainable Processes in the Circular Economy. Elsevier, pp. 83–122. https://doi.org/10.1016/B978-0-443-28886-9.00007-1

Küblböck, K., Tröster, B., Eigner, M., 2022. Hard facts and environmental impacts: An overview of the global iron and steel sector, ÖFSE Briefing Paper, No. 33. Austrian Foundation for Development Research, Vienna.

Kuila, U., McCarty, D.K., Derkowski, A., Fischer, T.B., Prasad, M., 2014. Total porosity measurement in gas shales by the water immersion porosimetry (WIP) method. Fuel 117, 1115–1129. https://doi.org/10.1016/j.fuel.2013.09.073

Kuila, U., Prasad, M., 2013. Specific surface area and pore-size distribution in clays and shales. Geophysical Prospecting 61, 341–362. https://doi.org/10.1111/1365-2478.12028

Kumar, M., Jena, S. and Patel, S.K. 2008. Characterization of properties and reduction behaviour of iron ores for application in sponge ironmaking. Mineral Processing and Extractive Metallurgy Review, 29(2), 118-129.

Li, A., Ding, W., Wang, R., He, J., Wang, X., Sun, Y., Gu, Y., Jiao, N., 2017. Petrophysical characterization of shale reservoir based on nuclear magnetic resonance (NMR) experiment: A case study of Lower Cambrian Qiongzhusi Formation in eastern Yunnan Province, South China. Journal of Natural Gas Science and Engineering 37, 29–38. https://doi.org/10.1016/j.jngse.2016.11.034

Li, F., Wang, R., Mao, L., Zhu, D., She, X., Guo, J., Lin, S., Yang, Y., 2022. Evaluation of solar radiation models on vertical surface for building photovoltaic applications in Beijing. IET Renewable Power Gen 16, 1792–1807. https://doi.org/10.1049/rpg2.12478

Li, Huamin, Li, Huigui, Wang, K., Liu, C., 2018. Effect of rock composition microstructure and pore characteristics on its rock mechanics properties. International Journal of Mining Science and Technology 28, 303–308. https://doi.org/10.1016/j.ijmst.2017.12.008

Li, J., Lu, S., Chen, G., Wang, M., Tian, S., Guo, Z., 2019. A new method for measuring shale porosity with low-field nuclear magnetic resonance considering non-fluid signals. Marine and Petroleum Geology 102, 535–543. https://doi.org/10.1016/j.marpetgeo.2019.01.013

Li, M., Wang, D., Shao, Z., 2020. Experimental study on changes of pore structure and mechanical properties of sandstone after high-temperature treatment using nuclear magnetic resonance. Engineering Geology 275, 105739. https://doi.org/10.1016/j.enggeo.2020.105739

Liu, L., Ge, Z., Zhou, Z., Li, Z., Deng, Q., 2024. Mineral composition, pore structure and mechanical properties of coal measure strata rocks: A case study of Pingdingshan Coalfield. Science of The Total Environment 952, 175944. https://doi.org/10.1016/j.scitotenv.2024.175944

Ma, B., Hu, Q., Yang, S., Yin, N., Qiao, H., Zhang, T., Meng, M., 2020. Multiple approaches to quantifying the Effective porosity of lacustrine shale oil reservoirs in Bohai Bay Basin, East China. Geofluids 2020, 1–13. https://doi.org/10.1155/2020/8856620

Ma, S., Jin, G., Sy, R., Kesserwan, H., 2018. Rock grain size prediction from NMR Measurement and digital rock modeling- experimental validation, in: All Days. Presented at the SPE Kingdom of Saudi Arabia Annual Technical Symposium and Exhibition, SPE, Dammam, Saudi Arabia, p. SPE-192220-MS. https://doi.org/10.2118/192220-MS

Madureira, N.L. (2012). The iron industry energy transition. Energy Policy, 50, 24-34. https://doi.org/10.1016/j.enpol.2012.03.003.

McNulty, T., Hazen, N., Park, S., 2022. Processing the ores of rare-earth elements. MRS Bulletin 47, 258–266. https://doi.org/10.1557/s43577-022-00288-4

Meiboom, S., Gill, D., 1958. Modified spin-echo method for measuring nuclear relaxation times. Review of scientific instruments 29, 688–691.

Mitchell, J., 2010. Nuclear magnetic resonance relaxation and diffusion in the presence of internal gradients: The effect of magnetic field strength. Phys. Rev. E 81. https://doi.org/10.1103/PhysRevE.81.026101

Mondal, I., Singh, K.H., 2023. Fluid substitution in NMR T2 distribution and resistivity independent saturation computation using synthetic capillary pressure data. Petroleum Research 8, 77–86. https://doi.org/10.1016/j.ptlrs.2022.03.004

Muwanguzi, A.J.B., Karasev, A.V., Byaruhanga, J.K. and Jönsson, P.G. (2012a). Characterisation of the Physical and Metallurgical Properties of Natural Iron Ore for Iron Production. International Scholarly Research Network (ISRN) Materials Science Volume, Article ID 147420, 9 p. https://doi.org/10.5402/2012/147420.

Muwanguzi, A.J.B., Karasev, A.V., Byaruhanga, J.K. and Jönsson, P.G. (2012b). Characterization of Chemical Composition and Microstructure of Natural Iron Ore from Muko Deposits. International Scholarly Research Network (ISRN) Materials Science Volume, Article ID 174803, 9 p. https://doi.org/10.5402/2012/174803.

Nilsen, B., Palmström, A., 2000. Engineering geology and rock engineering, handbook no. 2. Norwegian Soil and Rock Engineering Association, Oslo, Norway.

Niu, Q., Zhang, C., 2018. Joint inversion of NMR and SIP data to estimate pore size distribution of geomaterials. Geophysical Journal International 212, 1791–1805. https://doi.org/10.1093/gji/ggx501

O'Connor, J. M., Manuel, J. R., and Clout, J. M. F. (2000). Relationships between index test results and uniaxial compressive strength. Proceedings of the 4th International Conference on Geotechnical Engineering (GEOTECH-YEAR 2000), Bangkok, Thailand, 27–30 November 2000.

Obaje, N.G., 2009. Geology and Mineral Resources of Nigeria, Lecture Notes in Earth Sciences. Springer Berlin Heidelberg, Berlin, Heidelberg. https://doi.org/10.1007/978-3-540-92685-6.

Odigi, M.I., 2002. Geochemistry and geotectonic setting of migmatitic gneisses and amphibolites in the Okene-Lokoja area of southwestern Nigeria. Journal of mining and geology 38, 81–90.

Olade, M.A., 1978. Early Cretaceous basalt volcanism and initial continental rifting in Benue Trough, Nigeria. Nature 273, 458–459. https://doi.org/10.1038/273458a0

Olade, M.A., 1980. Precambrian metallogeny in West Africa. Geol Rundsch 69, 411–428. https://doi.org/10.1007/BF02104546

Olade, M.A., 2019. Geological Re-Evaluation of Nigeria's Iron Ore Deposits as Raw Materials for a

Viable Iron and Steel Industry. Achievers J. Sci. Research 2, 1–22.

Olatinsu, O.B., Olorode, D.O., Clennell, B., Esteban, L., Josh, M., 2017. Lithotype characterizations by Nuclear Magnetic Resonance (NMR): A case study on limestone and associated rocks from the eastern Dahomey Basin, Nigeria. Journal of African Earth Sciences 129, 701–712. https://doi.org/10.1016/j.jafrearsci.2017.02.005.

Oyedele, K., Oladele, S. and Salami, A., 2016. Geophysical investigation of banded iron ore mineralization at Ero, North–Central Nigeria. Materials and Geoenvironment, 63(2), 109-118. https://doi.org/10.1515/rmzmag-2016-0010.

Palchik, V., 2011. On the ratios between elastic modulus and uniaxial compressive strength of heterogeneous carbonate rocks. Rock Mech Rock Eng 44, 121–128. https://doi.org/10.1007/s00603-010-0112-7

Pamparana, G., Klein, B., Bergerman, M.G., 2024. Impact of the feed particle size distribution and its packing characteristics on compression comminution. Minerals Engineering 218, 108934. https://doi.org/10.1016/j.mineng.2024.108934

Peng, J., Wong, L.N.Y., Liu, G. and Teh, C.I. 2019. Influence of initial micro-crack damage on strength and micro-cracking behavior of an intrusive crystalline rock. Bull Eng Geol Environ 78, 2957–2971. https://doi.org/10.1007/s10064-018-1317-3.

Pereira, L., Schach, E., Tolosana-Delgado, R., Frenzel, M., 2023. All About Particles: Modelling Ore Behaviour in Mineral Processing. Elements 19, 359–364. https://doi.org/10.2138/gselements.19.6.359

Pereira, M.L., Pappalardo, L., Buono, G., Cueto, N., Vázquez-Calvo, C., Fort, R., Costa E Silva, M., Fernandes, I., Zanon, V., Amaral, P., 2025. A multi-method approach in the physical and mechanical assessment of lava rocks with distinct microstructure. Engineering Geology 346, 107907. https://doi.org/10.1016/j.enggeo.2025.107907

Rahaman, M.A., Ocan, O., 1978. On relationships in the Precambrian migmatic gneisses of Nigeria. Nigeria J. Min. Geol. 15, 23–32.

Rust, A.C., Cashman, K.V., 2011. Permeability controls on expansion and size distributions of pyroclasts: magma expansion and fragmentation. J. Geophys. Res. 116, n/a-n/a. https://doi.org/10.1029/2011JB008494

Ryshkewitch, E., 1953. Compression strength of porous sintered alumina and zirconia: 9th communication to ceramography. *Journal of the American Ceramic Society*, *36*(2), pp.65-68.

Salvini, S., Coletti, C., Maritan, L., Massironi, M., Balsamo, F., Mazzoli, C., 2023. Exploring the pore system of carbonate rocks through a multi-analytical approach. Environ Earth Sci 82, 564. https://doi.org/10.1007/s12665-023-11234-1

Santoro, L., Putzolu, F., Mondillo, N., Boni, M. and Herrington, R. (2022). Trace element geochemistry of iron-(oxy)-hydroxides in Ni(Co)-laterites: Review, new data and implications for ore forming processes. Ore Geology Reviews, 140, 104501. https://doi.org/10.1016/j.oregeorev.2021.104501.

Shah, M., Sahoo, K.L., Das, S.K., Das, G., 2020. Wear Mechanism of High Chromium White Cast Iron and Its Microstructural Evolutions During the Comminution Process. Tribol Lett 68, 77. https://doi.org/10.1007/s11249-020-01317-6

Siegesmund, S., Dürrast, H., 2011. Physical and Mechanical Properties of Rocks, in: Siegesmund, S., Snethlage, R. (Eds.), Stone in Architecture. Springer Berlin Heidelberg, Berlin, Heidelberg, pp. 97–225. https://doi.org/10.1007/978-3-642-14475-2_3

Somani, A., Nandi, T.K., Pal, S.K., Majumder, A.K., 2017. Pre-treatment of rocks prior to comminution – A critical review of present practices. International Journal of Mining Science and Technology 27, 339–348. https://doi.org/10.1016/j.ijmst.2017.01.013

Sparks, R.S.J., Annen, C., Blundy, J.D., Cashman, K.V., Rust, A.C., Jackson, M.D., 2019. Formation and dynamics of magma reservoirs. Phil. Trans. R. Soc. A. 377, 20180019. https://doi.org/10.1098/rsta.2018.0019

Sun, Y. Pan, A. Ma Y. and Chang, J. 2023. Extraction of alumina and silica from high-silica bauxite by sintering with sodium carbonate followed by two-step leaching with water and sulfuric acid. RSC Adv., 2023, 13, 23254. https://doi.org/10.1039/d3ra03362g.

Tan, S., Li, W., Li, H., Zhou, L. and Yu, M., 2026. Study on Effects of Mineral and Pore Characteristics on Mechanical Behavior and Acoustic Emission of Sandstone. *ACS omega*, *11*(9), pp.14729-14749. https://doi.org/10.1021/acsomega.5c10657.

Tavares, L.M., 2000. Role of particle microstructure in comminution, in: Massacci, P. (Ed.), Developments in

Mineral Processing, Oral Session. Elsevier, pp. C4-99. https://doi.org/10.1016/S0167-4528(00)80033-2.

Tijani, M.N. (2023). Geology of Nigeria. In: Faniran, A., Jeje, L.k., Fashae, O.A., Olusola, A.O. (eds) Landscapes and Landforms of Nigeria. World Geomorphological Landscapes. Springer, Cham. https://doi.org/10.1007/978-3-031-17972-3_1.

Timur, A., 1969. Pulsed Nuclear Magnetic Resonance Studies of Porosity, Movable Fluid, and Permeability of Sandstones. Journal of Petroleum Technology 21, 775–786. https://doi.org/10.2118/2045-PA

Ulusay, R. (Ed.), 2015. The ISRM Suggested Methods for Rock Characterization, Testing and Monitoring: 2007-2014. Springer International Publishing, Cham. https://doi.org/10.1007/978-3-319-07713-0

Ulusay, R., Hudson, J.A. (Eds.), 2007. The complete ISRM suggested methods for rock characterization, testing and monitoring: 1974–2006, In: Ulusay, R., Hudson, J.A. (Eds.), Suggested Methods Prepared by the Commission of Testing Methods. ed. (for the ISRM Turkish National Group), Kozam Ofset, Ankara, Turkey.

Ündül, Ö. (2012). Assessment of mineralogical and petrographic factors affecting petrophysical properties, strength and cracking processes of volcanic rocks. Eng. Geol. 2016, 210, 10 – 22.

Upadhyay, R.K., Venkatesh, A.S. and Roy, S. (2010). Mineralogical Characteristics of Iron Ores in Joda and Khondbond Areas in Eastern India with Implications on Beneficiation. Resource Geology Vol. 60, No. 2: 203–211. https://doi.org/10.1111/j.1751-3928.2010.00126.x.

Wang, M., Xie, J., Guo, F., Zhou, Y., Yang, X., Meng, Z., 2020. Determination of NMR T2 Cutoff and CT Scanning for Pore Structure Evaluation in Mixed Siliciclastic–Carbonate Rocks before and after Acidification. Energies 13, 1338. https://doi.org/10.3390/en13061338

Way, D., McKee, D., Pease, J., 2021. Comminution and Mineral Separation—Geological Input to Metallurgy. SEG Discovery 28–41. https://doi.org/10.5382/Geo-and-Mining-12

Williams, R.A., 1993. Processing problematic ores. Minerals Engineering 6, 809–816. https://doi.org/10.1016/0892-6875(93)90055-R

Wills, B.A., Atkinson, K., 1993. Some observations on the fracture and liberation of mineral assemblies. Minerals Engineering 6, 697–706. https://doi.org/10.1016/0892-6875(93)90001-4

Woakes, M., Rahaman, M.A., Ajibade, A.C., 1987. Some metallogenetic features of the Nigerian basement. Journal of African Earth Sciences (1983) 6, 655–664. https://doi.org/10.1016/0899-5362(87)90004-2

Xie, W.-Q., Liu, X.-L., Zhang, X.-P., Liu, Q.-S., Wang, E.-Z., 2025. A review of test methods for uniaxial compressive strength of rocks: Theory, apparatus and data processing. Journal of Rock Mechanics and Geotechnical Engineering 17, 1889–1905. https://doi.org/10.1016/j.jrmge.2024.05.003

Xu, S., Zhao, Y., Wang, M. and Shi, X. (2018). Quantification of Different Forms of Iron from Intact Soil Cores of Paddy Fields with Vis-NIR Spectroscopy. Soil Sci. Soc. Am. J., 82(6), 1497-1511. https://doi.org/10.2136/sssaj2018.01.0014.

Xu, Z., Lin, M., Jiang, W., Cao, G., Yi, Z., 2020. Identifying the comprehensive pore structure characteristics of a rock from 3D images. Journal of Petroleum Science and Engineering 187, 106764. https://doi.org/10.1016/j.petrol.2019.106764.

Yang, Z., Song, Z., Ding, X., Michele Victoire, M.N., Abdoul Wahab, A.M., Oumar, B., Yang, F., Yusuf Ibrahim, A., Gao, Z., Long, Z., 2025. Investigating slope stability of multiple stopes prone to instability in the Ziluoyi iron ore mining site. Sci Rep 15, 1900. https://doi.org/10.1038/s41598-025-85770-0

Yao, Y., Liu, D., 2012. Comparison of low-field NMR and mercury intrusion porosimetry in characterizing pore size distributions of coals. Fuel 95, 152–158. https://doi.org/10.1016/j.fuel.2011.12.039

Yao, Y., Liu, D., Cai, Y., Li, J., 2010a. Advanced characterization of pores and fractures in coals by nuclear magnetic resonance and X-ray computed tomography. Sci. China Earth Sci. 53, 854–862. https://doi.org/10.1007/s11430-010-0057-4

Yao, Y., Liu, D., Che, Y., Tang, D., Tang, S., Huang, W., 2010b. Petrophysical characterization of coals by low-field nuclear magnetic resonance (NMR). Fuel 89, 1371–1380. https://doi.org/10.1016/j.fuel.2009.11.005

Yao, Y., Liu, D., Liu, J., Xie, S., 2015. Assessing the Water Migration and Permeability of Large Intact Bituminous and Anthracite Coals Using NMR Relaxation Spectrometry. Transp Porous Med 107, 527–542. https://doi.org/10.1007/s11242-014-0452-y

Yao, Y., Liu, J., 2019. Petrophysical Characterization of the Pore Structure of Coal, in: Petrophysical Characterization and Fluids Transport in Unconventional Reservoirs. Elsevier, pp. 21–36. https://doi.org/10.1016/B978-0-12-816698-7.00002-4

Yao, Y., Sun, X., Zheng, S., Wu, H., Zhang, C., Liu, Y., Chang, Y., 2021. Methods for Petrological and Petrophysical Characterization of Gas Shales. Energy Fuels 35, 11061–11088. https://doi.org/10.1021/acs.energyfuels.1c01475

Zhai, H. Canbulat, I., Zhang, C., Watson, J. and Gao, M. 2025. Combined effects of discontinuities and intact rock on weak rock at various scales, Journal of Rock Mechanics and Geotechnical Engineering,17(12), 7676-7690. https://doi.org/10.1016/j.jrmge.2025.01.053.

Zhang, J., Tao, G., Huang, L., Yuan, L., 2010. Porosity models for determining the pore-size distribution of rocks and soils and their applications. Chin. Sci. Bull. 55, 3960–3970. https://doi.org/10.1007/s11434-010-4111-6

Zhang, Q.B., Zhao, J., 2014. Quasi-static and dynamic fracture behaviour of rock materials: phenomena and mechanisms. Int J Fract 189, 1–32. https://doi.org/10.1007/s10704-014-9959-z

Zhu, C., Zhu, E., Wang, B., Li, J., Yao, T., Zhang, Z., 2025. Effect of Porosity and Pore Size on the Axial Compressive Properties of Recycled Aggregate Concrete. Materials 18, 2830. https://doi.org/10.3390/ma18122830

Zuo, W., Shi, F., 2016. Ore impact breakage characterisation using mixed particles in wide size range. Minerals Engineering 86, 96–103. https://doi.org/10.1016/j.mineng.2015.12.007